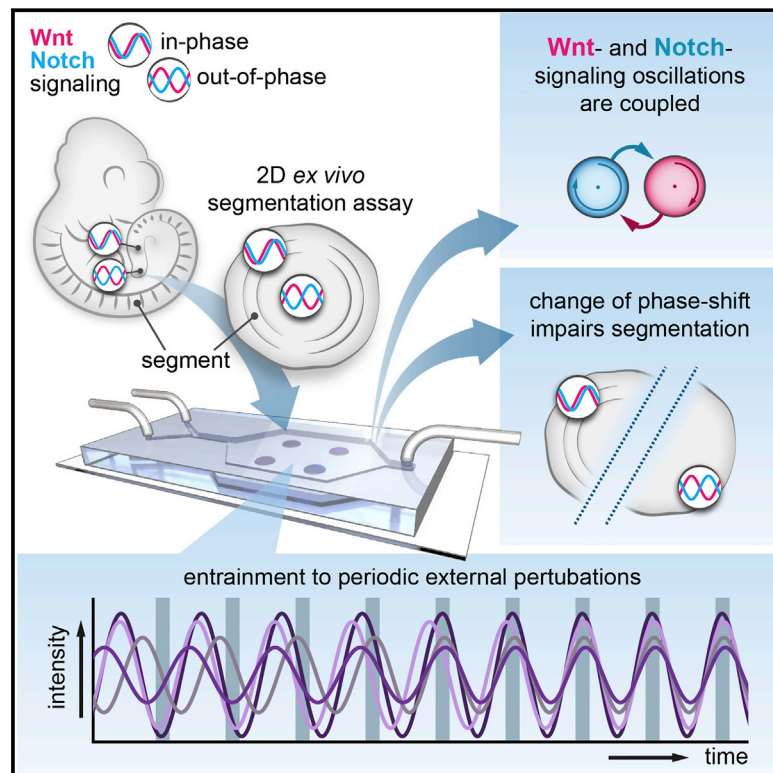


Modulation of Phase Shift between Wnt and Notch Signaling Oscillations Controls Mesoderm Segmentation

Graphical Abstract



Authors

Katharina F. Sonnen, Volker M. Lauschke, Julia Uraji, ..., Paul François, Christoph A. Merten, Alexander Aulehla

Correspondence

aulehla@embl.de

In Brief

The relative timing between oscillatory Wnt and Notch signaling is critical for the segmentation of mouse embryo mesoderm.

Highlights

- Wnt and Notch signaling wave dynamics differ within segmenting mouse mesoderm
- Entraining oscillations by microfluidics allows external control of the dynamics
- Oscillatory Wnt and Notch signaling networks are coupled at the level of dynamics
- Relative timing of Wnt and Notch signaling oscillations is critical for segmentation



Modulation of Phase Shift between Wnt and Notch Signaling Oscillations Controls Mesoderm Segmentation

Katharina F. Sonnen,^{1,2} Volker M. Lauschke,^{1,4} Julia Uraji,¹ Henning J. Falk,¹ Yvonne Petersen,¹ Maja C. Funk,¹ Mathias Beaupeux,³ Paul François,³ Christoph A. Merten,² and Alexander Aulehla^{1,5,*}

¹Developmental Biology Unit

European Molecular Biology Laboratory, 69117 Heidelberg, Germany

²Genome Biology Unit

European Molecular Biology Laboratory, 69117 Heidelberg, Germany

³Department of Physics, McGill University, Montréal, Canada

⁴Present address: Department of Physiology and Pharmacology, Karolinska Institutet, Stockholm, Sweden

⁵Lead Contact

*Correspondence: aulehla@embl.de

<https://doi.org/10.1016/j.cell.2018.01.026>

SUMMARY

How signaling dynamics encode information is a central question in biology. During vertebrate development, dynamic Notch signaling oscillations control segmentation of the presomitic mesoderm (PSM). In mouse embryos, this molecular clock comprises signaling oscillations of several pathways, i.e., Notch, Wnt, and FGF signaling. Here, we directly address the role of the relative timing between Wnt and Notch signaling oscillations during PSM patterning. To this end, we developed a new experimental strategy using microfluidics-based entrainment that enables specific control of the rhythm of segmentation clock oscillations. Using this approach, we find that Wnt and Notch signaling are coupled at the level of their oscillation dynamics. Furthermore, we provide functional evidence that the oscillation phase shift between Wnt and Notch signaling is critical for PSM segmentation. Our work hence reveals that dynamic signaling, i.e., the relative timing between oscillatory signals, encodes essential information during multicellular development.

INTRODUCTION

Periodic segmentation of mesoderm into somites, the precursors of vertebrae, is controlled by a molecular clock, which in mouse embryos includes ultradian (period ~2 hr) oscillations in Notch, Wnt, and FGF pathway activity (Dequéant and Pourquié, 2008; Oates et al., 2012; Soza-Ried et al., 2014). Several studies have addressed the linkage between the oscillating pathways, and multiple molecular connections leading to cross-talk between the signaling networks have been suggested previously (e.g., Aulehla et al., 2003; Aulehla et al., 2008; Niwa et al., 2007; Niwa et al., 2011; Pourquié, 2011; Wahl et al., 2007). However, the functional relationship between the pathways at

the level of oscillations remains an open question, primarily because it cannot be resolved by continuous interference with any of the pathways using chemical or genetic approaches (e.g., Aulehla et al., 2003; Aulehla et al., 2008; Niwa et al., 2007; Niwa et al., 2011; Sonnen and Aulehla, 2014; Wahl et al., 2007).

Notch signaling oscillations have been shown to be slightly phase shifted from one cell to the next along the anteroposterior axis in a spatially graded manner, and hence, oscillations generate periodic Notch activity waves that traverse the embryo from posterior to anterior, as visualized using real-time imaging (Aulehla et al., 2008; Delaune et al., 2012; Masamizu et al., 2006; Soroldoni et al., 2014). In posterior PSM regions, FGF and Notch signaling oscillate in phase (Dequéant et al., 2006), while Wnt signaling oscillations occur out of phase relative to Notch and FGF signaling oscillations (Aulehla et al., 2003; Dequéant et al., 2006; Krol et al., 2011). Moreover, unlike Wnt signaling oscillations (Hirata et al., 2004; Niwa et al., 2007), both the Notch and the FGF signaling oscillations depend on the transcriptional repressor *Hes7*, a core component of the segmentation clock, suggesting that oscillations of Notch and FGF signaling constitute outputs of a single clock mechanism (Harima and Kageyama, 2013). Between oscillatory Notch and FGF signals, it has been shown that *Fgf* signaling needs to be periodically shut off in newly forming segments within anterior PSM to allow active Notch signaling to induce expression of the differentiation marker *Mesp2* in this region. These data collectively indicate that the differential regulation of individual oscillatory pathways may be critical for segmentation (Niwa et al., 2011; Oginuma et al., 2008).

However, whether Notch/FGF and Wnt signaling dynamics are linked and whether there is a function at the level of relative oscillation rhythms remains unknown and could not be directly addressed so far. We have therefore established a real-time knockin reporter mouse line enabling quantification of endogenous Wnt signaling oscillations and, critically, established a microfluidic system, which allowed us to control the rhythms of Wnt and Notch signaling oscillations during mouse segmentation.



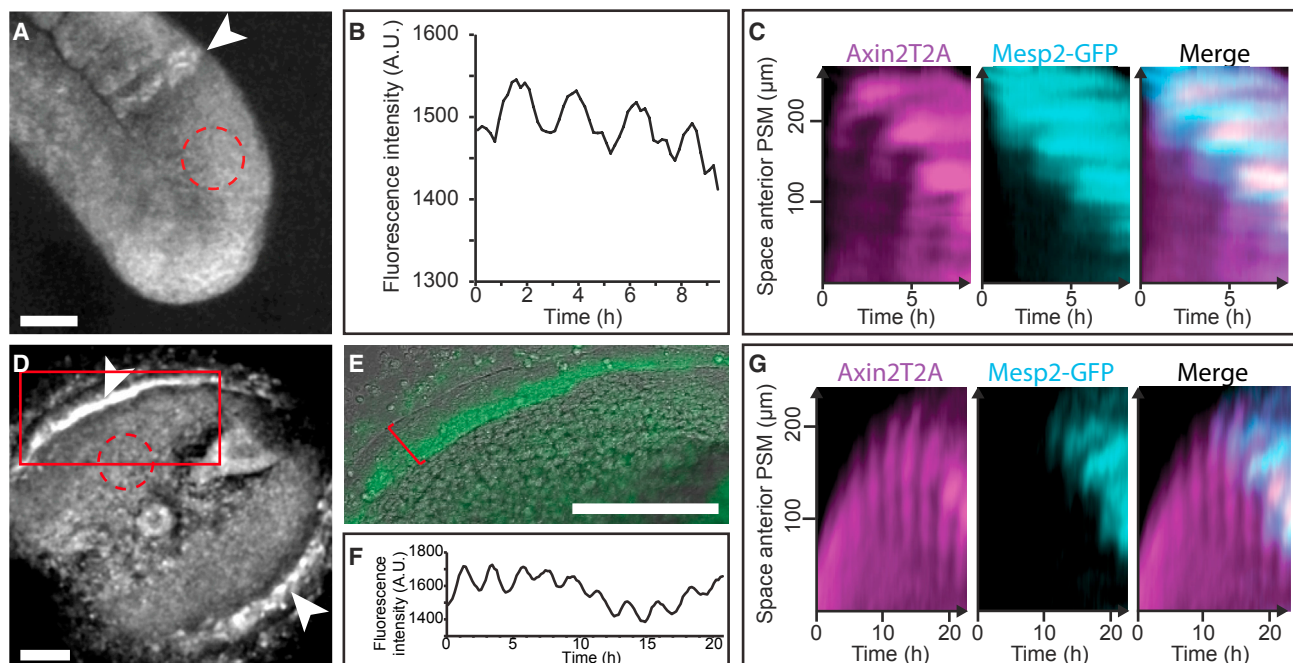


Figure 1. Real-Time Visualization of Wnt Signaling Oscillations during Mesodermal Patterning

(A) Snapshot of a representative Axin2T2A *in vivo* real-time imaging experiment (also shown in [Movie S1](#)). Dorsal view of the posterior PSM and recently formed somites. White arrow indicates stripe of Axin2T2A expression in the posterior half of newly forming somite. Scale bar, 100 μ m.

(B) Axin2T2A reporter signal in region of interest in (A) (ROI, red circle) is plotted over time.

(C) Intensity kymograph established from real-time imaging of an Axin2T2A and Mesp2-GFP double-positive PSM. Axin2T2A fluorescence (left panel), Mesp2-GFP fluorescence (middle panel), and merge of the two channels (right panel) are shown. After registration of real-time movie, kymograph was generated by averaging signal intensity over width of a 70 μ m wide line. Note that in newly forming segments, Axin2T2A expression alternates with Mesp2-GFP expression.

(D) Snapshot of a representative *ex vivo* Axin2T2A reporter cell culture assay (also shown in [Movie S2](#)). White arrowhead indicates stripe of expression in forming segment. Scale bar, 100 μ m.

(E) Red box in (D) is magnified (green) and overlaid with the corresponding brightfield image (gray) illustrating Axin2T2A reporter expression stripe in the posterior half of newly forming segment. Red line highlights formed segment. Scale bar, 100 μ m.

(F) Axin2T2A reporter signal in ROI (red circle in [D]) is plotted over time. Note long-lasting Axin2T2A reporter oscillations.

(G) Intensity kymograph established from real-time imaging of an Axin2T2A and Mesp2-GFP double-positive *ex vivo* culture. Axin2T2A fluorescence (left panel), Mesp2-GFP fluorescence (middle panel), and merge of the two channels (right panel) are shown. To generate kymograph, signal intensity was averaged over width of a 70 μ m wide line.

RESULTS

Generation of a Dynamic Wnt Signaling Reporter

While dynamic FGF and Notch signaling reporters have been published previously ([Aulehla et al., 2008](#); [Masamizu et al., 2006](#); [Niwa et al., 2011](#)), such reporters to quantify endogenous Wnt signaling activity oscillations were not yet available. Therefore, we generated knockin real-time reporter mouse lines for *Axin2*, a bona fide direct Wnt signaling target gene ([Aulehla et al., 2003](#); [Jho et al., 2002](#); [Lustig et al., 2002](#)). This was done by inserting sequences encoding a destabilized reporter, i.e., Venus-PEST or Luciferase-PEST, into the *Axin2* locus separated by a 2A-site ([Szymczak et al., 2004](#)) ([Figure S1A](#)).

In vivo fluorescence imaging of the Axin2-T2A-VenusPEST reporter mouse line, hereafter termed Axin2T2A, revealed gene activity oscillations within the PSM, with a period of 142.8 ± 14.4 SD min ([Figures 1A, 1B, and S1B](#) and [Movie S1](#)). In newly forming segments, Axin2T2A reliably showed a stable expression that was restricted to the posterior half of the

segment, spatially alternating with the differentiation marker Mesp2 expressed in anterior PSM ([Figures 1A and 1C](#) and [Movie S1](#)), thus reflecting endogenous expression patterns ([Aulehla et al., 2003](#); [Saga et al., 1997](#)). Furthermore, *ex vivo* two-dimensional (2D) segmentation assays ([Lauschke et al., 2013](#)) recapitulated Axin2T2A oscillations within a (quasi-) monolayer PSM (mPSM, [Figures 1D–1F](#) and [Movie S2](#)) with a period identical to *in vivo* oscillations ([Figure S1B](#)).

Thus, we successfully established and validated ([Figures S1C–S1E](#)) a Wnt signaling reporter mouse line that enables real-time quantification of Axin2 expression dynamics during mesoderm segmentation.

Phase Shift between Wnt and Notch Signaling Oscillations Changes along PSM

Employing this fluorescent reporter Axin2T2A and *ex vivo* mPSM cultures, we performed in-depth analyses of Wnt signaling dynamics during segmentation ([Figure 2A](#)). Axin2T2A oscillations resulted in periodic waves of high velocity that slowed down

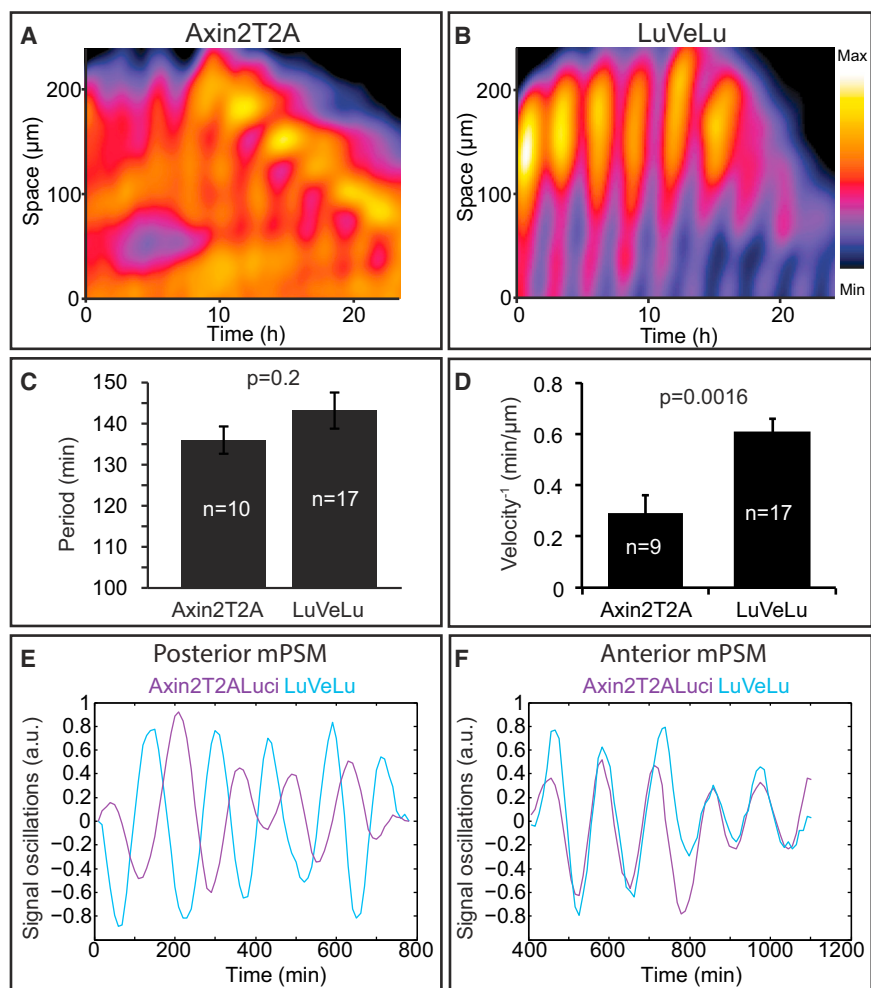


Figure 2. Quantification of Wnt and Notch Signaling Reporter Oscillations Reveals Changing Phase Shift from Posterior to Anterior mPSM

(A and B) Fluorescence intensity kymographs of *ex vivo* cell culture assays using Wnt signaling reporter Axin2T2A (A) or Notch signaling reporter LuVeLu (B) (the same kymographs and brightfield images of the cultures are shown in Figure S2). Fluorescence intensity is color-coded independently for each kymograph.

(C) Quantification of posterior oscillation periods in Axin2T2A or LuVeLu reveals no significant difference ($p = 0.2$).

(D) Inverse velocity was quantified based on phase kymographs. LuVeLu waves were significantly slower than Axin2T2A waves ($p = 0.0016$). For comparison, quantification of the fourth wave during the segmentation cycle of the 2D *ex vivo* culture (Lauschke et al., 2013) is depicted (see Figure S2G for further analysis). Error bars in (C) and (D) indicate SEM.

(E) Quantification (detrrending, normalization) of Axin2T2A-Luciferase (magenta) and LuVeLu (cyan) reporter activity in *ex vivo* mPSM assay at beginning of culture. Note that only posterior PSM cells are used to generate *ex vivo* cultures so that oscillations detected at beginning of cultivation period represent exclusively posterior PSM cells (Lauschke et al., 2013). (Reporter signal was quantified in region of interest [yellow circle] shown in Figure S2H.)

(F) Quantification of detrrended, normalized Axin2T2A-Luciferase and LuVeLu reporter signal in anterior region of *ex vivo* assay using Axin2T2A-Luciferase (magenta) and LuVeLu (cyan) double-positive samples. (Oscillations were obtained by determining reporter signal along the line in the kymograph of anterior mPSM in Figure S2I.) This reveals that preceding the abrupt decrease in Axin2T2A wave velocity, which marks future segment boundaries (see Figure 1C and 1G for onset of *Mesp2*), Axin2T2A and LuVeLu oscillate in phase.

abruptly in the most anterior mPSM (periphery of *ex vivo* culture) ($n = 38/52$ waves). Confirming the *in vivo* data (Figure 1C), the region exhibiting slow Axin2T2A waves spatiotemporally overlapped with expression onset of *Mesp2* (Saga et al., 1997) (Figure 1G).

To quantitatively compare Wnt and Notch signaling oscillation dynamics, we analyzed Axin2T2A and Notch signaling reporter oscillations in the mPSM region spatiotemporally preceding segment formation, corresponding to the mPSM domain exhibiting fast Axin2 waves. Importantly, dynamics of the Notch target gene *lunatic fringe* (*Lfng*) (Figure 2B), visualized by the reporter mouse line LuVeLu (Aulehla et al., 2008), differed markedly from Axin2T2A dynamics (Figure 2A). While Axin2T2A and LuVeLu waves showed similar periods (Figure 2C), LuVeLu waves traversed the mPSM significantly slower than Axin2 waves (Figures 2D and S2A–S2G). Additional quantification with a knockin line we generated for *Lfng*, *Lfng*-T2A-VenusPEST, showed oscillation dynamics that were indistinguishable from LuVeLu, indicating that our quantification was not biased by the choice of reporter strategy (data not shown). As Axin2T2A

and LuVeLu waves exhibit different velocities, these waves necessarily change their phase relation along the mPSM.

To directly assess the modulation of the phase shift within the PSM, we performed simultaneous imaging of *ex vivo* cultures expressing both Notch and Wnt reporter (i.e., LuVeLu and luciferase-tagged reporter Axin2T2A-Luciferase). In agreement with previous static data (Aulehla et al., 2003; Dequéant et al., 2006; Krol et al., 2011), Wnt and Notch signaling reporters oscillated out of phase in posterior mPSM (center of *ex vivo* culture) (Figures 2E and S2H). In contrast, we found that in the anterior mPSM (periphery of *ex vivo* culture), Wnt and Notch signaling oscillations occurred in-phase, in a region preceding the abrupt slowing down of Axin2T2A-Luciferase waves—and, hence, the onset of *Mesp2* expression (Figures 2F and S2I, see also Figure 1F).

These findings are, in principle, compatible with a mechanism in which the local phase shift between oscillatory Wnt and Notch signaling in the PSM encodes information for mesoderm segmentation. Thus, we decided to develop an experimental system that allows for directly testing the possible function of this local Wnt/Notch phase shift in PSM segmentation.

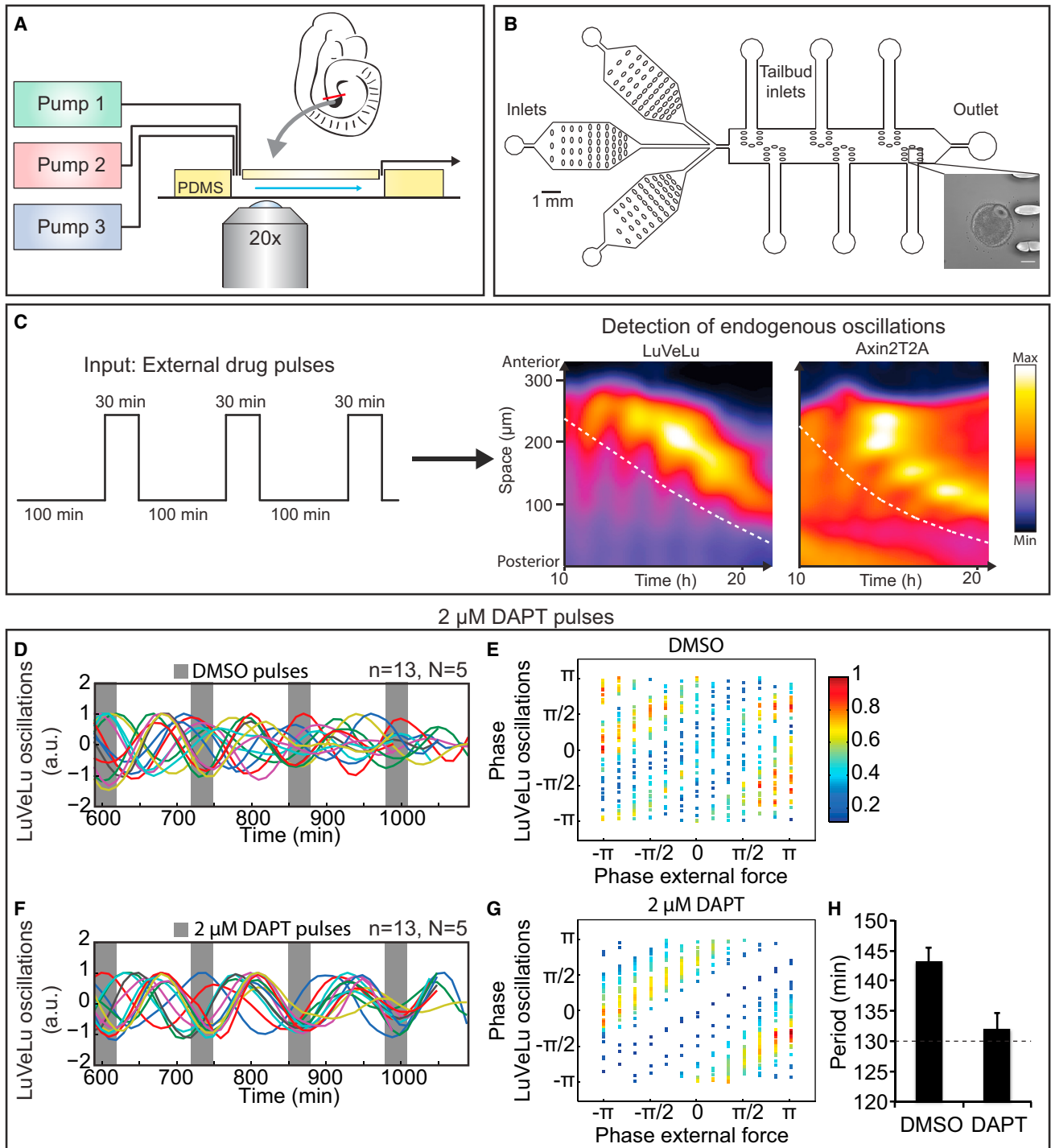


Figure 3. Microfluidic System Enables Entrainment of Signaling Oscillations to a Periodic External Force

(A) Schematic representation of the microfluidic setup consisting of a PDMS chip, perfused using several pumps, enabling on-chip mPSM *ex vivo* cultures combined with simultaneous real-time imaging.

(B) General chip design showing one of the two cultivation chambers present on a microfluidic chip (top view). The depth of the chip is approximately 300 μm . Inset depicts brightfield image of mPSM culture within microfluidic chip (scale bar of inset, 100 μm).

(C) Scheme of experimental setup. Periodic pulses of signaling pathway modulator were applied to mPSM *ex vivo* cultures, and endogenous signaling pathway oscillations were detected. Dashed lines in representative fluorescence intensity kymographs of LuVeLu and Axin2T2A mPSM cultures depict the region corresponding to anterior mPSM, in which oscillations were measured for further analysis.

(legend continued on next page)

Microfluidics-Based Approach to Entrain Segmentation Clock Oscillations

With the goal of specifically controlling the endogenous rhythms of Wnt and Notch signaling oscillations, we established a microfluidic system and combined it with the 2D segmentation assay. This enables us to temporally control culture conditions while monitoring endogenous signaling oscillations by simultaneous fluorescence imaging (Figure 3A). The microfluidic chip consists of two chambers with up to three inlets each, enabling cultivation of multiple 2D *ex vivo* assays (Figure 3B). We first verified that tissues cultured on chip under perfusion conditions developed quantitatively comparable to off-chip standard 2D *ex vivo* assays (mPSM) in terms of oscillations of LuVeLu or Axin2T2A and induction of the differentiation marker Mesp2-GFP in a periphery-to-center direction (data not shown).

Next, to control oscillations of Notch and Wnt signaling, we aimed to synchronize either of the signaling pathways to periodic external perturbations (referred to as “external force” [Pikovsky et al., 2001]) by periodic application of small molecules that modulate either Notch or Wnt signaling, respectively (Figure 3C). Synchronization is defined as a stable phase relationship between two periodic signals—in this case, the rhythm of endogenous oscillations of Wnt or Notch signaling and that of small molecule pulses (Pikovsky et al., 2001). According to entrainment theory, a periodic external force can synchronize an oscillator most efficiently if their frequencies are similar, i.e., at small frequency detuning. In this case, a small perturbation is sufficient (Pikovsky et al., 2001). Hence, we applied pulses at intervals of 130 min (Figure 3C)—close to the endogenous oscillation period—and used relatively low doses of DAPT (2 μ M), a gamma-secretase and, thus, Notch pathway inhibitor, or of CHIR99021 (Chiron, 5 μ M), a GSK3 inhibitor leading to Wnt pathway activation. Infusion of drugs into the microfluidic chamber was monitored by detection of the fluorescent dye Cascade Blue (Movie S3). For the analysis of signaling dynamics, Notch and Wnt signaling oscillations were analyzed in the anterior mPSM region preceding segmentation (Figure 3C).

Strikingly, periodic DAPT pulses synchronized endogenous Notch signaling oscillations to the external DAPT rhythm (Figure 3D–3H and Data S1A). Accordingly, the endogenous Notch signaling oscillation phase showed a stable relationship with the phase of external force pulses (Figure 3G), and the periods of endogenous oscillations and external pulses matched (Figure 3H). In contrast, control DMSO pulses did not synchronize oscillations (Figures 3D, 3E, 3H, and Data S1A). Similarly, we found that pulses of Chiron entrained endogenous Wnt signaling oscillations and thus that the rhythm of endogenous Axin2T2A oscillations matched the rhythm of external pulses of Chiron (Figures S3A–S3D and Data S1D). Importantly, periodic perturbations with either Chiron or DAPT did not elicit apparent changes of overall

signaling levels, i.e., signaling amplitude or absolute signaling activity (Figure S4). Thus, we have established an experimental approach using microfluidic entrainment by periodic external perturbations that allows us to specifically control the *rhythm* of endogenous Wnt or Notch signaling oscillations within segmenting tissue in 2D segmentation assays.

Wnt and Notch Signaling Oscillations Are Coupled

Using this approach, we first investigated whether Wnt and Notch signaling oscillations are linked. To this end, we analyzed what effect the entrainment of Notch signaling oscillations has on Wnt signaling oscillations and vice versa. Interestingly, we found that upon entrainment of Notch signaling oscillations with DAPT, Wnt signaling oscillations were also synchronized (Figures 4A–4E and Data S1B). Similarly, entrainment of Wnt signaling oscillations with Chiron led to synchronized Notch signaling oscillations relative to the external pulses (Figures S3E–S3H and Data S1C). Furthermore, the phase relationship between the two oscillating pathways was maintained in the anterior mPSM even after the experimental alteration. Accordingly, Wnt and Notch pathways continued to show in-phase oscillations in anterior mPSM, preceding segment formation, as observed in control embryos (DAPT: Figure 4F, Chiron: Figure S3I). These in-phase oscillations were accompanied with stepwise segmentation and the onset of Axin2 expression in posterior halves of forming segments (DAPT: Figure 4G, Chiron: Figure S3J).

Together, these results provide direct functional evidence that Notch and Wnt signaling oscillations are coupled within the PSM, which is reflected in the ability to mutually synchronize each other upon entrainment of one signaling pathway.

Changing Rhythm between Wnt and Notch Signaling Oscillations in Anterior PSM

Notably, however, due to this coupling between Wnt and Notch signaling oscillations, entrainment of one oscillatory pathway did not change their phase relationship and thus did not allow us to directly examine the role of the Wnt and Notch oscillation phase shift. We reasoned that if entrainment to the external rhythm was robust, it might be possible to control the Wnt/Notch phase shift by entraining both signaling pathways to two external rhythms in parallel. We therefore analyzed the effect on the Wnt/Notch phase shift, when Chiron and DAPT were applied in alternating or simultaneous pulses. The phase shift between Wnt and Notch signaling was quantified in the anterior mPSM region (see Figure 3C), which in control embryos shows in-phase Wnt and Notch signaling oscillations, preceding segmentation.

When we applied Chiron and DAPT in alternating pulses, each for 30 min at 130 min intervals, endogenous Wnt and Notch signaling oscillations in anterior mPSM synchronized to the rhythm of Chiron and DAPT, respectively; as previously,

(D–H) Entrainment of LuVeLu oscillations to periodic pulses of the Notch inhibitor DAPT (2 μ M):

(D and F) Quantification of (detrended, normalized) LuVeLu signal in anterior mPSM reveals oscillations in control (D) and DAPT-treated samples (F). Experiments (N = independent experiments, n = individual samples) were combined using the external force (gray bars) as an objective time reference.

(E and G) Phase-phase plots of the phase relation between endogenous rhythm (LuVeLu) and external periodic force (control: DMSO pulses [E], treatment: DAPT pulses [G]) reveals stable phase relationship for entrained DAPT samples. Density of points within the plots is color-coded.

(H) Mean period of oscillations in (D) and (F) (see full timeseries data in Data S1A) was quantified. Error bars indicate SEM.

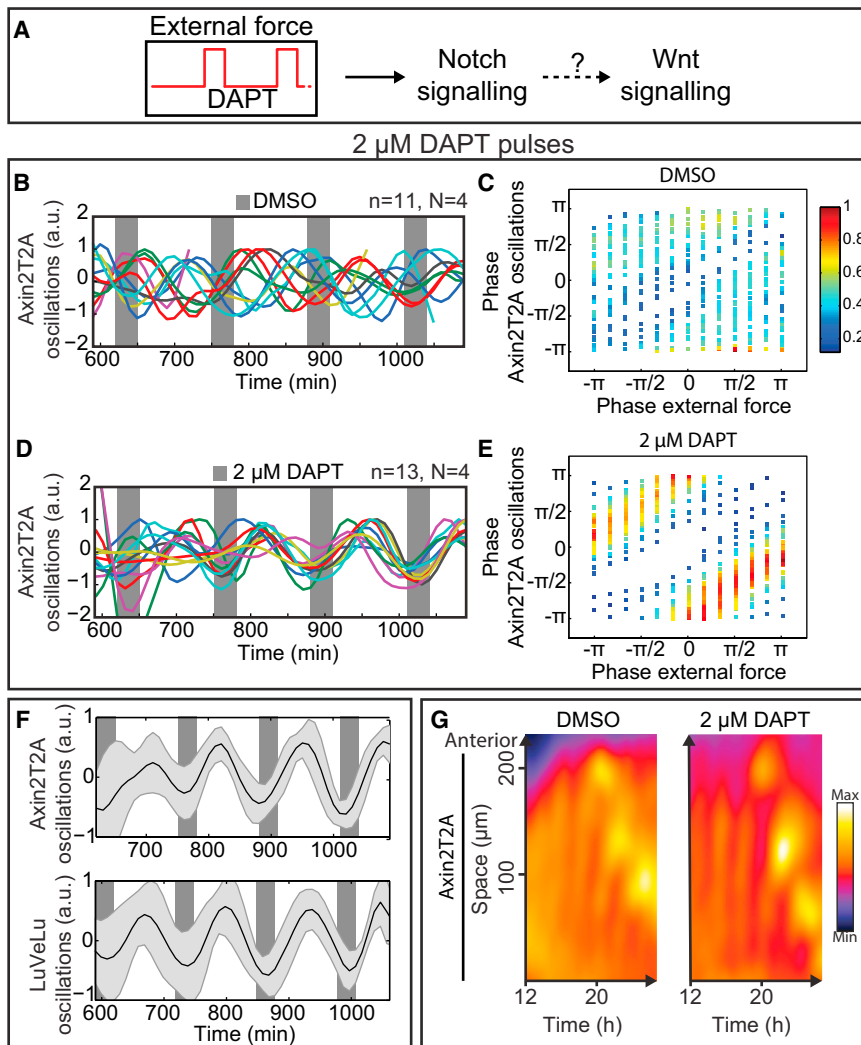


Figure 4. Wnt Signaling Oscillations Are Linked to Notch Signaling Oscillations

(A) Scheme of experimental setup. Periodic pulses of Notch signaling inhibitor DAPT ($2 \mu\text{M}$) were applied to mPSM *ex vivo* cultures and endogenous Axin2T2A oscillations were detected.

(B–E) Entrainment of Axin2T2A oscillations to periodic pulses of the Notch inhibitor DAPT ($2 \mu\text{M}$): (B and D) Quantification of (detrended, normalized) Axin2T2A signal in anterior mPSM reveals oscillations in control (B) and DAPT-treated samples (D). Experiments (N = independent experiments, n = individual samples) were combined using the external force (gray bars) as an objective time reference.

(C and E) Phase-phase plots of the phase relation between endogenous rhythm (Axin2T2A) and external periodic force (control: DMSO pulses [C], treatment: DAPT pulses [E]). Density of points within the plots is color-coded.

(F) Mean reporter activity (black line) and SD (gray shading) of Axin2T2A oscillations shown in (D) and LuVeLu oscillations shown in Figure 3F reveal in-phase oscillations in anterior mPSM upon entrainment with DAPT pulses (N = independent experiments, n = individual samples).

(G) Representative Axin2T2A fluorescence intensity kymographs of DMSO control- (left panel) and DAPT-treated mPSM *ex vivo* cultures (right panel). Fluorescence intensity is color-coded. (See Data S1B for full timeseries data.)

Phase Relationship between Wnt and Notch Signaling Oscillations in Anterior PSM Is Critical for Proper Segmentation

Our approach therefore enabled us for the first time to directly address whether the local phase shift between Wnt and

DMSO pulses did not synchronize oscillations (Data S2A and S2B). Under these conditions, Wnt and Notch signaling oscillations occurred in-phase in anterior mPSM (Figures 5A–5D), as in control samples (Figure 2F). In contrast, when we applied external drug pulses simultaneously using the same, otherwise unchanged treatment conditions (again for 30 min and at 130 min intervals), Wnt and Notch signaling oscillations now occurred in anti-phase in the anterior mPSM (Figures 5E–5H, Data S2C and S2D). Notably, similarly to single-pathway entrainment experiments, concomitant entrainment of both Notch and Wnt signaling oscillations did not cause an observable effect on *overall* signaling levels: neither amplitude nor absolute levels of Notch and Wnt signaling reporters were significantly changed in comparison to control samples (Figure S5).

Thus, by entraining both pathways in parallel, we were able to overcome the intrinsic coupling between the pathways. In effect, this approach enabled us to specifically change the relative timing, i.e., the phase shift, between multiple oscillating signaling pathways.

Notch signaling oscillations in anterior PSM would be of *functional* significance.

Entrainment with alternating pulses of Chiron and DAPT, which led to in-phase Wnt and Notch signaling oscillations in anterior mPSM (Figure 5D), did not cause an observable phenotype in segmentation compared to DMSO controls (Figure 6). However, entraining the endogenous rhythms with simultaneous pulses of Chiron and DAPT, resulting in anti-phase Wnt and Notch signaling oscillations in anterior mPSM (Figure 5H), led to a robust segmentation phenotype (Figure 6). First, we found that the arrest of oscillations in anterior mPSM did not occur on time, and thus, mPSM cells maintained their oscillatory state significantly longer compared to control mPSM cells (Figures 6A–6C). Furthermore, anti-phase Wnt and Notch signaling oscillations impaired physical segment formation (Figures 6D–6F). This is the first direct evidence that experimental modulation of the Wnt/Notch phase shift is sufficient to control the arrest of oscillations in the anterior PSM, hence perturbing mesoderm segmentation.

To further characterize the observed phenotype, we performed a molecular analysis of several segment markers upon

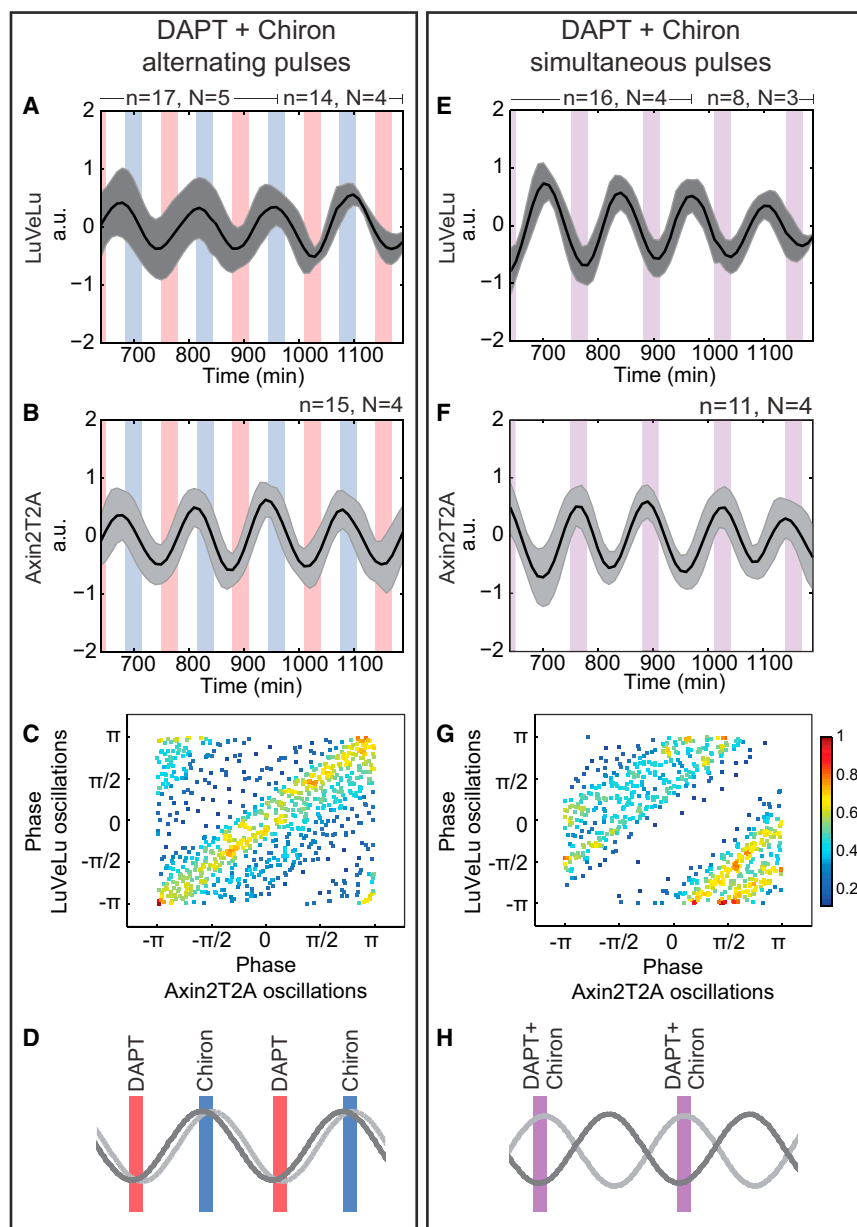


Figure 5. Experimental Modulation of Phase Shift between Wnt and Notch Signaling Oscillations Using Microfluidics

(A–H) Quantification (detrrending, normalization) of LuVeLu (A and E) or Axin2T2A (B and F) signals in mPSM samples cultured either with alternating (A–C) or simultaneous pulses (E–G) of 2 μ M DAPT and 5 μ M Chiron. All measurements were done in anterior mPSM (see Figure 3C). Individual experiments were aligned to each other using external perturbations as objective time reference. Black line depicts mean, gray shading depicts SD of combined samples (N = independent experiments, n = individual samples). (C and G) Phase-phase plots of LuVeLu versus Axin2T2A oscillations upon alternating (C) or simultaneous DAPT/Chiron pulses (G). Density of points is color-coded. (D and H) Schematic representation of phase relationship between LuVeLu and Axin2T2A oscillations in anterior mPSM upon alternating (D) or simultaneous (H) DAPT/Chiron pulses. (See Data S2 for full timeseries of treatment with both simultaneous and alternating drug pulses.)

tion in samples entrained with simultaneous pulses of Chiron and DAPT. Thus, this indicates that despite Mesp2 expression, segment formation and segment polarity were severely impaired when the phase shift between Wnt and Notch signaling oscillations was experimentally altered (Figures 6D, 6F, and S6). Combined, our data provide functional evidence that the phase shift between Wnt and Notch oscillations is a critical factor during mesoderm segmentation.

DISCUSSION

Here, we addressed the fundamental question of how information for spatio-temporal patterning during embryonic development is encoded based on dynamic, oscillatory signals. To specifically

address the role of rhythm between Wnt and Notch signaling oscillations, we developed a novel experimental approach that combines quantitative real-time measurements with the ability to experimentally control the timing between Wnt and Notch signaling oscillations.

entrainment. We found that the somite segmentation marker Mesp2, which is controlled by FGF and Wnt signaling gradients but is independent of oscillatory Notch or FGF signaling (Aulehla et al., 2008; Niwa et al., 2011; Oginuma et al., 2008; Saga, 2012), and its downstream target Ripply2 (Morimoto et al., 2007) were expressed in samples entrained with alternating or simultaneous pulses of Chiron and DAPT (Figures S6A and S6B). Moreover, real-time imaging using a Mesp2 reporter showed that expression occurred on time even when the phase shift between Wnt and Notch signaling oscillations was experimentally altered (Figures S6C–S6H). In contrast, we found that posterior-half segment markers, such as Axin2 (Figures 1E and S6I–S6L) and the homeobox gene Uncx4.1 (Figures S6A and S6B) (Mansouri et al., 1997; Neidhardt et al., 1997), lost their expres-

address the role of rhythm between Wnt and Notch signaling oscillations, we developed a novel experimental approach that combines quantitative real-time measurements with the ability to experimentally control the timing between Wnt and Notch signaling oscillations.

Entrainment of the Segmentation Clock Reveals Cross-Talk between Wnt and Notch Signaling Oscillations

Using this quantitative approach, we first revealed that Notch and Wnt signaling oscillations are functionally linked during mouse mesoderm segmentation. Previous findings indicated that the clock mechanism of Wnt signaling oscillations might differ from that of Notch signaling oscillations, as for instance knockout of the core clock component Hes7 abolished

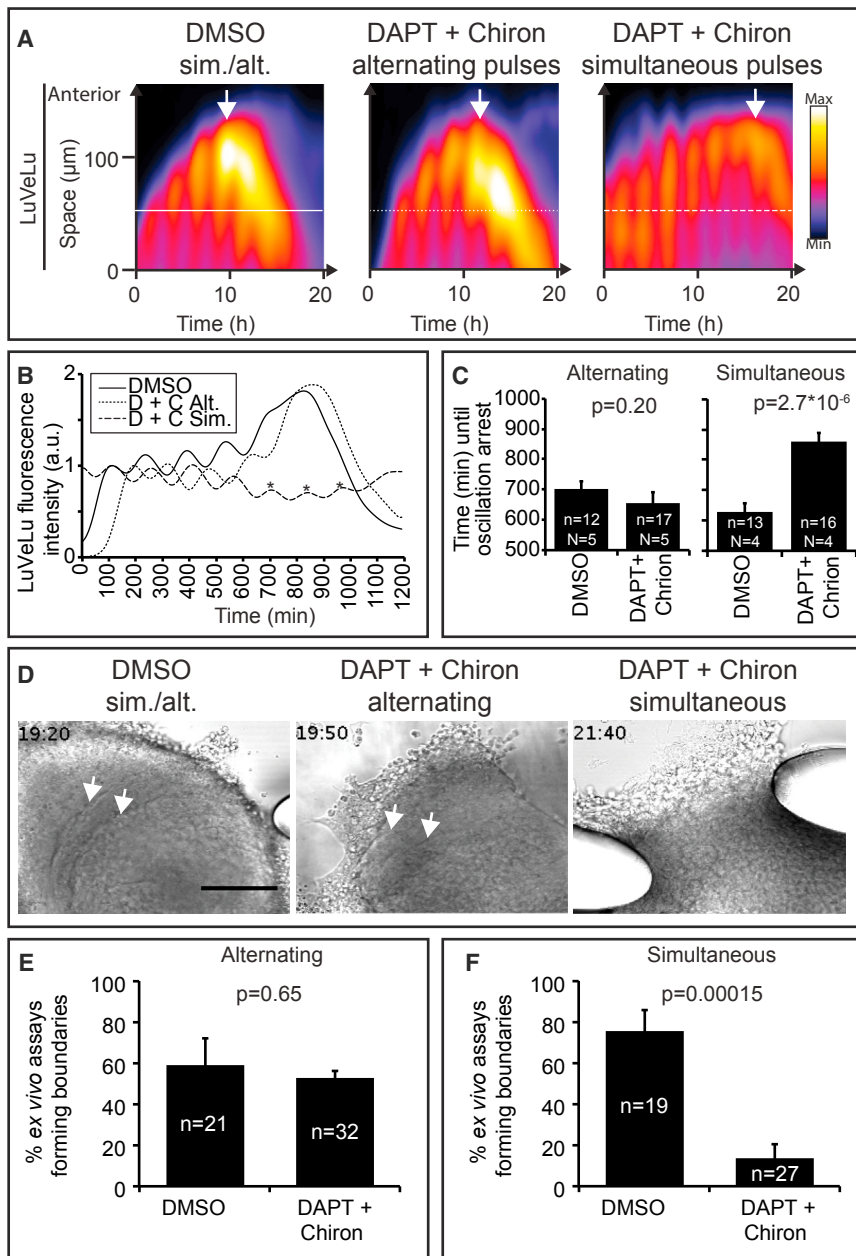


Figure 6. Modulation of Phase Shift between Wnt and Notch Signaling Oscillations Delays Oscillation Arrest and Impairs Proper mPSM Segmentation

(A) Representative fluorescence intensity kymographs of *ex vivo* cultures using the Notch reporter LuVeLu are depicted for samples treated either with DMSO pulses (left panel), alternating (middle panel, “alt.”), or simultaneous pulses (right panel, “sim.”) of 2 μM DAPT and 5 μM Chiron. Fluorescence intensity is color-coded. White arrows mark time point of oscillation arrest.

(B) Quantification of LuVeLu fluorescence intensity in a particular region in anterior mPSM (white lines in [A]). Individual samples were normalized to the fluorescence intensity of the first oscillation peak within each time-series. Asterisks indicate additional cycles of oscillations in the sample treated with simultaneous pulses of DAPT/Chiron.

(C) Quantification of time until oscillation arrest in experiments with either alternating (left panel) or simultaneous external force pulses (right panel). N = independent experiments, n = individual samples. Error bars denote SEM.

(D) Representative brightfield images of *ex vivo* cultures showing segment formation in samples treated either with DMSO (left panel) or alternating DAPT/Chiron pulses (middle panel). In contrast, physical boundary formation was absent in samples entrained with simultaneous DAPT/Chiron pulses (right panel).

(E and F) Quantification of *ex vivo* cultures forming physical boundaries in experiments treated with alternating (E) or simultaneous (F) DAPT/Chiron pulses compared to DMSO control. Error bars denote SEM.

oscillations being synchronized relative to this external, rhythmic perturbation. Vice versa, synchronization of Notch signaling oscillations by pulses of Notch signaling inhibitor also resulted in synchronized Wnt signaling oscillations.

While our entrainment approach provides evidence that Notch and Wnt signaling oscillations are mutually coupled, it is interesting to point out that endogenously, the phase shift between

Notch and FGF signaling oscillations, whereas Wnt signaling oscillations were still detectable (Hirata et al., 2004). While previous data clearly indicated a tight interconnection between the Notch/FGF and Wnt pathways at the genetic level (Aulehla et al., 2008; Dubrulle et al., 2001; Wahl et al., 2007), it remained unclear whether these pathways are linked at the level of their oscillatory activity.

Using novel knockin Axin2 reporter mouse lines combined with the microfluidic entrainment approach, we now reveal that Wnt and Notch signaling are indeed coupled at the level of oscillation rhythm. We found that entrainment of Wnt signaling oscillations using external periodic pulses of a small molecule activator of canonical Wnt signaling led, over time, also to Notch signaling

oscillations being synchronized relative to this external, rhythmic perturbation. Vice versa, synchronization of Notch signaling oscillations by pulses of Notch signaling inhibitor also resulted in synchronized Wnt signaling oscillations. While our entrainment approach provides evidence that Notch and Wnt signaling oscillations are mutually coupled, it is interesting to point out that endogenously, the phase shift between Wnt and Notch signaling changes depending on the PSM region. Oscillations occur out of phase in posterior PSM and tail bud (Aulehla et al., 2003; Dequéant et al., 2006; Krol et al., 2011) (Figure 2E), while cells in anterior PSM show in-phase oscillations, preceding segmentation. From a theoretical viewpoint, the entrainment phase between two coupled oscillators can be influenced by various parameters, such as coupling strength and entrainment range (Granada et al., 2013), and it remains unknown if any of these parameter changes along the PSM. Likewise, it will be critical to test the role of signaling gradients present in the PSM and to test whether and how these modulate the Wnt/Notch phase shift in space and time.

Relative Timing between Wnt and Notch Signaling Oscillations Controls Mesoderm Segmentation

The ability to control the rhythms of Wnt and Notch signaling oscillations *individually* opened up the possibility to extend the entrainment approach to specifically alter the timing between these oscillating pathways. This was indeed achieved by entraining both Wnt and Notch signaling *simultaneously*, which enabled us to overcome their endogenous link and to experimentally alter the timing, i.e., phase shift, between Wnt and Notch signaling oscillations. It is critical to point out that we could not detect any effect on overall signaling levels upon periodic entrainment with either single or multiple small molecules (Figures S4 and S5). This means that the experimental conditions, i.e., alternating versus simultaneous entrainment, differ visibly only at the level of temporal relationship between Wnt and Notch signaling oscillations.

Notably, the entrainment outcome, i.e., Wnt/Notch phase shift, varied along the PSM: while alternating pulses of DAPT and Chiron robustly led to in-phase oscillations in the anterior PSM (Figure 5), the Wnt/Notch phase shift in more posterior PSM regions was found to be out of phase (see kymographs in Figure 6A) even after entrainment. While the underlying reason for this outcome remains to be investigated, several possibilities can be discussed. Of note, entrainment is performed in a highly complex and, importantly, spatially non-uniform context. This is seen most evidently at the level of Notch oscillation frequency, which gradually changes, i.e., decreases, along the PSM. Therefore, it follows that detuning, i.e., the frequency difference, between internal oscillators and external periodic drug pulses differs along the PSM, as well. It is known from entrainment theory that detuning is a critical parameter with pronounced effect not only on the synchronization outcome, but also on the phase of entrainment between internal and external oscillators (Bordyugov et al., 2015; Granada et al., 2013; Pikovsky et al., 2001). The precise role detuning plays during PSM entrainment needs to be further investigated. In addition, PSM cells are coupled at multiple levels; intercellular coupling to neighboring cells via Notch signaling has been shown in multiple systems (Horikawa et al., 2006; Jiang et al., 2000; Masamizu et al., 2006), and in addition, in this study, we revealed coupling at the level of signaling pathways, i.e., Wnt and Notch signaling oscillations are linked. It is also possible that coupling is spatially non-uniform, as we find, for instance, that the endogenous Wnt/Notch phase shift changes along the PSM. Future work will be necessary to investigate this complex, multi-level coupling along the entire PSM in order to disentangle its role during entrainment but more generally during the PSM patterning process *per se*.

In this study, we focused our analysis on the anterior PSM region preceding segmentation, as the entrainment was robust, resulting in either in-phase or out-of-phase oscillations depending on the entrainment regime applied (Figure 5). Using this approach, we provide experimental evidence for a functional role of the phase shift between Wnt and Notch signaling oscillations. We found that the ability to maintain an oscillatory PSM state and proper segmentation is controlled by the phase shift between Wnt and Notch signaling oscillations in the anterior PSM. This suggests a role of oscillation dynamics of multiple

signaling pathways during PSM patterning and development, such as an oscillation-based feedback on oscillation arrest and PSM cell differentiation.

Role of Oscillation Phase Shift between Wnt and Notch Signaling in Segmentation Models

Currently, the most widely accepted model how PSM oscillations arrest and segmentation is induced is the “clock and wavefront” model. In this model, segmentation clock oscillations stop when cells pass a “wavefront,” which in turn has been experimentally linked to FGF and Wnt signaling gradients in the PSM (Aulehla et al., 2008; Bajard et al., 2014; Dubrulle et al., 2001; Dunty et al., 2008; Sawada et al., 2001). In the clock and wavefront framework, cells can be kept in an oscillatory state by altering the wavefront, e.g., when FGF and Wnt signaling levels are increased (Aulehla et al., 2008; Dubrulle et al., 2001). However, in our experiments, we maintained cells in an oscillatory state for an extended time even though we neither changed overall Wnt signaling levels (Figure S5) nor directly manipulated FGF signaling levels. In agreement, we found that timing of expression of *Mesp2*, which is controlled by signaling gradients and does not require a functioning clock (Aulehla et al., 2008; Niwa et al., 2011; Oginuma et al., 2008; Saga, 2012), was not altered upon entrainment. Furthermore, *Mesogenin1*, a downstream target of Wnt signaling and a marker for signaling gradients along the PSM (Wittler et al., 2007; Yoon and Wold, 2000), was expressed in a qualitatively similar manner upon entrainment (Figure S6A). Thus, these findings indicate that it is possible to experimentally decouple the role of the phase shift in controlling the arrest of oscillations and the role of signaling gradients in controlling the onset of *Mesp2* and *Mesogenin* expression. A finer dissection of the precise contribution and interplay of oscillation phase shift and signaling gradients is now necessary and will require further development of the current experimental approach allowing, for instance, to control phase shift and signaling gradients in a spatially refined manner.

Previously, we found that oscillation dynamics of Notch signaling are predictive of segment size, and we proposed that wave dynamics might be decoded relative to a second oscillator (Lauschke et al., 2013, its supplement and Beaupoux et al., 2016, for a theoretical study). Here, we provide evidence that Wnt and Notch signaling oscillations, which are linked at the level of their oscillations, occur in phase specifically in the anterior PSM preceding segmentation; and second, we demonstrate that the phase shift between Wnt and Notch oscillations is functionally important. Combined, these findings are compatible with Wnt signaling operating as a reference oscillator to decode Notch signaling wave dynamics in time and space.

Relative Timing of Dynamic Signals as General Principle of Information Encoding

Dynamic signal encoding based on relative timing of oscillatory or pulsatile signals has been studied and applied in a wide range of scientific disciplines ranging from engineering (Andrewes, 1996; Oppenheim et al., 1997) to neuroscience (Bi and Poo, 1998; Hashemi et al., 2010). Dynamic signal encoding has also been investigated at the level of cellular signaling activities

and transcription factor dynamics (e.g., Albeck et al., 2013; Ashall et al., 2009; Batchelor et al., 2008; Dolmetsch et al., 1997; Lin et al., 2015; Nelson et al., 2004; Purvis et al., 2012; Santos et al., 2007; Toettcher et al., 2013) (reviewed in Sonnen and Aulehla, 2014). Also in these contexts, the role of *relative* timing between dynamic signals is being increasingly revealed. For example, Lin et al. (2015) demonstrated the functional importance of the *relative timing* between pulsatile transcription factors in controlling gene expression in *Saccharomyces cerevisiae*. Our study advances this emerging picture, as we provide evidence that dynamic information encoding based on the relative timing between oscillatory signal transduction pathways also operates at multicellular scale during mammalian development.

As more cellular activities are being monitored quantitatively and at cellular resolution, the examples of pulsatile and oscillatory signals being identified will surely continue to increase over the coming years. A remaining common challenge will be to find experimental strategies to decipher the specific function encoded at the level of signaling dynamics (see also Imayoshi et al., 2013; Soza-Ried et al., 2014; Tay et al., 2010). Here, we show that by using an entrainment approach combined with dynamic reporter systems, it is now feasible to experimentally control the timing between endogenously linked oscillatory signaling machineries even in a more complex framework of embryonic development.

It is an exciting prospect to compare the roles and principles linked to oscillatory and phase-shifted signaling in these diverse cellular and multicellular dynamical systems.

STAR★METHODS

Detailed methods are provided in the online version of this paper and include the following:

- KEY RESOURCES TABLE
- CONTACT FOR REAGENT AND RESOURCE SHARING
- EXPERIMENTAL MODEL AND SUBJECT DETAILS
 - Mouse lines
- METHOD DETAILS
 - Transgenesis, mouse strains and animal work
 - mPSM ex vivo culture on microfluidic chip
 - In situ hybridization
 - Laser scanning microscopy
 - Bioluminescence imaging
- QUANTIFICATION AND STATISTICAL ANALYSIS
 - Image and data processing
 - Generation and analysis of kymographs
 - Analysis of simultaneous imaging of Axin2T2A-Luci and LuVeLu
 - Analysis of entrainment of oscillations in anterior mPSM
- DATA AND SOFTWARE AVAILABILITY

SUPPLEMENTAL INFORMATION

Supplemental Information includes six figures, two data sets, and three movies and can be found with this article online at <https://doi.org/10.1016/j.cell.2018.01.026>.

ACKNOWLEDGMENTS

We thank members of the Aulehla and Merten groups and Takashi Hiragi for discussion and comments on the manuscript. We thank Henning Falk for designing the graphical abstract. We thank Antonio Politi (Group Jan Ellenberg, EMBL Heidelberg) for providing the macro *Pipeline Constructor* for real-time imaging of microfluidic experiments. We are grateful to Jana Kress, Ivica Lehotska, and Nobuko Tsuchida-Straeten for technical assistance and to Nirupama Ramanathan for advice during establishment of microfluidic assay. This work was supported by EMBL Imaging and Animal core facilities. The Mesp2-GFP line was kindly provided by Yumiko Saga (NIG, Mishima). The Hes7-knockout line was kindly provided by Yasumasa Bessho. K.F.S. has been supported by a research fellowship from the Swiss National Science Foundation (SNSF) and by the EMBL Interdisciplinary Postdoc Program under Marie Curie COFUNDII Actions. M.B. has been supported by a Clifford Wong fellowship. P.F. is supported by the Natural Sciences and Engineering Research Council of Canada (NSERC) and a Simons Foundation Investigator Award in the Mathematical Modeling of Living Systems. This work received funding from the European Research Council under an ERC starting grant agreement n. 639343 to A.A.

AUTHOR CONTRIBUTIONS

K.F.S. designed the project, developed the microfluidic system, performed entrainment experiments, analyzed data, and wrote the manuscript. V.M.L. designed the project, generated and characterized knockin reporters, quantified wave dynamics, and wrote the manuscript. J.U. performed simultaneous reporter quantifications using Axin2T2A-Luci and LuVeLu. H.J.F. performed real-time imaging quantifications and data analysis. Y.P. generated chimeric animals. M.C.F. characterized the knockin reporters. M.B. and P.F. contributed to data analysis and project design. C.A.M. designed the project, envisaged the microfluidic approach to study cell signaling, and supervised development of the microfluidic platform. A.A. designed and supervised the project and wrote the manuscript. All authors discussed and contributed to the manuscript.

DECLARATION OF INTERESTS

The authors declare no competing interests.

Received: April 21, 2017

Revised: September 26, 2017

Accepted: January 18, 2018

Published: February 22, 2018

REFERENCES

- Albeck, J.G., Mills, G.B., and Brugge, J.S. (2013). Frequency-modulated pulses of ERK activity transmit quantitative proliferation signals. *Mol. Cell* 49, 249–261.
- Andrewes, W.J.H. (1996). The Quest for Longitude. In *Proceedings of the Longitude Symposium*, Harvard University, Cambridge, Massachusetts, November 4–6, 1993, W.J.H. Andrewes, ed. (Harvard University Collection of Historical Scientific Instruments), p. 437.
- Ashall, L., Horton, C.A., Nelson, D.E., Paszek, P., Harper, C.V., Sillitoe, K., Ryan, S., Spiller, D.G., Unitt, J.F., Broomhead, D.S., et al. (2009). Pulsatile stimulation determines timing and specificity of NF- κ B-dependent transcription. *Science* 324, 242–246.
- Aulehla, A., Wehrle, C., Brand-Saberi, B., Kemler, R., Gossler, A., Kanzler, B., and Herrmann, B.G. (2003). Wnt3a plays a major role in the segmentation clock controlling somitogenesis. *Dev. Cell* 4, 395–406.
- Aulehla, A., Wiegand, W., Baubet, V., Wahl, M.B., Deng, C., Taketo, M., Lewandoski, M., and Pourquié, O. (2008). A beta-catenin gradient links the clock and wavefront systems in mouse embryo segmentation. *Nat. Cell Biol.* 10, 186–193.

- Bajard, L., Morelli, L.G., Ares, S., Pécraux, J., Jülicher, F., and Oates, A.C. (2014). Wnt-regulated dynamics of positional information in zebrafish somitogenesis. *Development* *141*, 1381–1391.
- Batchelor, E., Mock, C.S., Bhan, I., Loewer, A., and Lahav, G. (2008). Recurrent initiation: a mechanism for triggering p53 pulses in response to DNA damage. *Mol. Cell* *30*, 277–289.
- Beaupeux, M., and François, P. (2016). Positional information from oscillatory phase shifts: insights from in silico evolution. *Phys Biol* *13*, 036009.
- Bessho, Y., Sakata, R., Komatsu, S., Shiota, K., Yamada, S., and Kageyama, R. (2001). Dynamic expression and essential functions of Hes7 in somite segmentation. *Genes Dev.* *15*, 2642–2647.
- Bi, G.Q., and Poo, M.M. (1998). Synaptic modifications in cultured hippocampal neurons: dependence on spike timing, synaptic strength, and postsynaptic cell type. *J. Neurosci.* *18*, 10464–10472.
- Bordyugov, G., Abraham, U., Granada, A., Rose, P., Imkeller, K., Kramer, A., and Herzl, H. (2015). Tuning the phase of circadian entrainment. *J. R. Soc. Interface* *12*, 20150282.
- Delaune, E.A., François, P., Shih, N.P., and Amacher, S.L. (2012). Single-cell-resolution imaging of the impact of Notch signaling and mitosis on segmentation clock dynamics. *Dev. Cell* *23*, 995–1005.
- Dequéant, M.-L., and Pourquié, O. (2008). Segmental patterning of the vertebrate embryonic axis. *Nat. Rev. Genet.* *9*, 370–382.
- Dequéant, M.L., Glynn, E., Gaudenz, K., Wahl, M., Chen, J., Mushegian, A., and Pourquié, O. (2006). A complex oscillating network of signaling genes underlies the mouse segmentation clock. *Science* *314*, 1595–1598.
- Dolmetsch, R.E., Lewis, R.S., Goodnow, C.C., and Healy, J.I. (1997). Differential activation of transcription factors induced by Ca²⁺ response amplitude and duration. *Nature* *386*, 855–858.
- Dubrulle, J., McGrew, M.J., and Pourquié, O. (2001). FGF signaling controls somite boundary position and regulates segmentation clock control of spatio-temporal Hox gene activation. *Cell* *106*, 219–232.
- Dunty, W.C., Jr., Biris, K.K., Chalamalasetty, R.B., Taketo, M.M., Lewandoski, M., and Yamaguchi, T.P. (2008). Wnt3a/beta-catenin signaling controls posterior body development by coordinating mesoderm formation and segmentation. *Development* *135*, 85–94.
- Eilers, P.H., and Goeman, J.J. (2004). Enhancing scatterplots with smoothed densities. *Bioinformatics* *20*, 623–628.
- El Debs, B., Utharala, R., Balyasnikova, I.V., Griffiths, A.D., and Merten, C.A. (2012). Functional single-cell hybridoma screening using droplet-based microfluidics. *Proc. Natl. Acad. Sci. USA* *109*, 11570–11575.
- Glynn, E.F., Chen, J., and Mushegian, A.R. (2006). Detecting periodic patterns in unevenly spaced gene expression time series using Lomb-Scargle periodograms. *Bioinformatics* *22*, 310–316.
- Granada, A.E., Bordyugov, G., Kramer, A., and Herzl, H. (2013). Human chronotypes from a theoretical perspective. *PLoS ONE* *8*, e59464.
- Harima, Y., and Kageyama, R. (2013). Oscillatory links of Fgf signaling and Hes7 in the segmentation clock. *Curr. Opin. Genet. Dev.* *23*, 484–490.
- Hashemi, R.H., Bradley, W.G., and Lisanti, C.J. (2010). MRI: The Basics, Third edition (Lippincott Williams & Wilkins).
- Hirata, H., Bessho, Y., Kokubu, H., Masamizu, Y., Yamada, S., Lewis, J., and Kageyama, R. (2004). Instability of Hes7 protein is crucial for the somite segmentation clock. *Nat. Genet.* *36*, 750–754.
- Horikawa, K., Ishimatsu, K., Yoshimoto, E., Kondo, S., and Takeda, H. (2006). Noise-resistant and synchronized oscillation of the segmentation clock. *Nature* *441*, 719–723.
- Imayoshi, I., Isomura, A., Harima, Y., Kawaguchi, K., Kori, H., Miyachi, H., Fujiwara, T., Ishidate, F., and Kageyama, R. (2013). Oscillatory control of factors determining multipotency and fate in mouse neural progenitors. *Science* *342*, 1203–1208.
- Jho, E.H., Zhang, T., Domon, C., Joo, C.K., Freund, J.N., and Costantini, F. (2002). Wnt/beta-catenin/Tcf signaling induces the transcription of Axin2, a negative regulator of the signaling pathway. *Mol. Cell. Biol.* *22*, 1172–1183.
- Jiang, Y.-J., Aerne, B.L., Smithers, L., Haddon, C., Ish-Horowicz, D., and Lewis, J. (2000). Notch signalling and the synchronization of the somite segmentation clock. *Nature* *408*, 475–479.
- Krol, A.J., Roellig, D., Dequéant, M.-L., Tassy, O., Glynn, E., Hattem, G., Mushegian, A., Oates, A.C., and Pourquié, O. (2011). Evolutionary plasticity of segmentation clock networks. *Development* *138*, 2783–2792.
- Lauschke, V.M., Tsiariris, C.D., François, P., and Aulehla, A. (2013). Scaling of embryonic patterning based on phase-gradient encoding. *Nature* *493*, 101–105.
- Lin, Y., Sohn, C.H., Dalal, C.K., Cai, L., and Elowitz, M.B. (2015). Combinatorial gene regulation by modulation of relative pulse timing. *Nature* *527*, 54–58.
- Lustig, B., Jerchow, B., Sachs, M., Weiler, S., Pietsch, T., Karsten, U., van de Wetering, M., Clevers, H., Schlag, P.M., Birchmeier, W., and Behrens, J. (2002). Negative feedback loop of Wnt signaling through upregulation of conductin/axin2 in colorectal and liver tumors. *Mol. Cell. Biol.* *22*, 1184–1193.
- Mansouri, A., Yokota, Y., Wehr, R., Copeland, N.G., Jenkins, N.A., and Gruss, P. (1997). Paired-related murine homeobox gene expressed in the developing sclerotome, kidney, and nervous system. *Dev. Dyn.* *210*, 53–65.
- Masamizu, Y., Ohtsuka, T., Takashima, Y., Nagahara, H., Takenaka, Y., Yoshikawa, K., Okamura, H., and Kageyama, R. (2006). Real-time imaging of the somite segmentation clock: revelation of unstable oscillators in the individual presomitic mesoderm cells. *Proc. Natl. Acad. Sci. USA* *103*, 1313–1318.
- Morimoto, M., Kiso, M., Sasaki, N., and Saga, Y. (2006). Cooperative Mesp activity is required for normal somitogenesis along the anterior-posterior axis. *Dev. Biol.* *300*, 687–698.
- Morimoto, M., Sasaki, N., Oginuma, M., Kiso, M., Igarashi, K., Aizaki, K., Kanno, J., and Saga, Y. (2007). The negative regulation of Mesp2 by mouse Ripply2 is required to establish the rostro-caudal patterning within a somite. *Development* *134*, 1561–1569.
- Nagai, T., Ibata, K., Park, E.S., Kubota, M., Mikoshiba, K., and Miyawaki, A. (2002). A variant of yellow fluorescent protein with fast and efficient maturation for cell-biological applications. *Nat. Biotechnol.* *20*, 87–90.
- Neidhardt, L.M., Kispert, A., and Herrmann, B.G. (1997). A mouse gene of the paired-related homeobox class expressed in the caudal somite compartment and in the developing vertebral column, kidney and nervous system. *Dev. Genes Evol.* *207*, 330–339.
- Nelson, D.E., Ihekweaba, A.E., Elliott, M., Johnson, J.R., Gibney, C.A., Foreman, B.E., Nelson, G., See, V., Horton, C.A., Spiller, D.G., et al. (2004). Oscillations in NF-kappaB signaling control the dynamics of gene expression. *Science* *306*, 704–708.
- Niwa, Y., Masamizu, Y., Liu, T., Nakayama, R., Deng, C.-X., and Kageyama, R. (2007). The initiation and propagation of Hes7 oscillation are cooperatively regulated by Fgf and notch signaling in the somite segmentation clock. *Dev. Cell* *13*, 298–304.
- Niwa, Y., Shimojo, H., Isomura, A., González, A., Miyachi, H., and Kageyama, R. (2011). Different types of oscillations in Notch and Fgf signaling regulate the spatiotemporal periodicity of somitogenesis. *Genes Dev.* *25*, 1115–1120.
- Oates, A.C., Morelli, L.G., and Ares, S. (2012). Patterning embryos with oscillations: structure, function and dynamics of the vertebrate segmentation clock. *Development* *139*, 625–639.
- Oginuma, M., Niwa, Y., Chapman, D.L., and Saga, Y. (2008). Mesp2 and Tbx6 cooperatively create periodic patterns coupled with the clock machinery during mouse somitogenesis. *Development* *135*, 2555–2562.
- Oppenheim, A.V., Willsky, A.S., and Nawab, S.H. (1997). Signals & systems, Second Edition (Upper Saddle River, N.J.: Prentice Hall).
- Pikovsky, A., Rosenblum, M., and Kurths, J. (2001). Synchronization: a universal concept in nonlinear sciences (Cambridge: Cambridge University Press).
- Pourquié, O. (2011). Vertebrate segmentation: from cyclic gene networks to scoliosis. *Cell* *145*, 650–663.
- Purvis, J.E., Karhohs, K.W., Mock, C., Batchelor, E., Loewer, A., and Lahav, G. (2012). p53 dynamics control cell fate. *Science* *336*, 1440–1444.

- Saga, Y. (2012). The mechanism of somite formation in mice. *Curr. Opin. Genet. Dev.* 22, 331–338.
- Saga, Y., Hata, N., Koseki, H., and Taketo, M.M. (1997). *Mesp2*: a novel mouse gene expressed in the presegmented mesoderm and essential for segmentation initiation. *Genes Dev.* 11, 1827–1839.
- Santos, S.D.M., Verwee, P.J., and Bastiaens, P.I.H. (2007). Growth factor-induced MAPK network topology shapes Erk response determining PC-12 cell fate. *Nat. Cell Biol.* 9, 324–330.
- Sawada, A., Shinya, M., Jiang, Y.J., Kawakami, A., Kuroiwa, A., and Takeda, H. (2001). Fgf/MAPK signalling is a crucial positional cue in somite boundary formation. *Development* 128, 4873–4880.
- Schindelin, J., Arganda-Carreras, I., Frise, E., Kaynig, V., Longair, M., Pietzsch, T., Preibisch, S., Rueden, C., Saalfeld, S., Schmid, B., et al. (2012). Fiji: an open-source platform for biological-image analysis. *Nat. Methods* 9, 676–682.
- Sonnen, K.F., and Aulehla, A. (2014). Dynamic signal encoding—from cells to organisms. *Semin. Cell Dev. Biol.* 34, 91–98.
- Soroldoni, D., Jörg, D.J., Morelli, L.G., Richmond, D.L., Schindelin, J., Jülicher, F., and Oates, A.C. (2014). Genetic oscillations. A Doppler effect in embryonic pattern formation. *Science* 345, 222–225.
- Soza-Ried, C., Öztürk, E., Ish-Horowicz, D., and Lewis, J. (2014). Pulses of Notch activation synchronise oscillating somite cells and entrain the zebrafish segmentation clock. *Development* 141, 1780–1788.
- Szymczak, A.L., Workman, C.J., Wang, Y., Vignali, K.M., Dilioglou, S., Vanin, E.F., and Vignali, D.A. (2004). Correction of multi-gene deficiency in vivo using a single ‘self-cleaving’ 2A peptide-based retroviral vector. *Nat. Biotechnol.* 22, 589–594.
- Tay, S., Hughey, J.J., Lee, T.K., Lipniacki, T., Quake, S.R., and Covert, M.W. (2010). Single-cell NF- κ B dynamics reveal digital activation and analogue information processing. *Nature* 466, 267–271.
- Toettcher, J.E., Weiner, O.D., and Lim, W.A. (2013). Using optogenetics to interrogate the dynamic control of signal transmission by the Ras/Erk module. *Cell* 155, 1422–1434.
- Wahl, M.B., Deng, C., Lewandoski, M., and Pourquié, O. (2007). FGF signaling acts upstream of the NOTCH and WNT signaling pathways to control segmentation clock oscillations in mouse somitogenesis. *Development* 134, 4033–4041.
- Wittler, L., Shin, E.H., Grote, P., Kispert, A., Beckers, A., Gossler, A., Werber, M., and Herrmann, B.G. (2007). Expression of *Msgn1* in the presomitic mesoderm is controlled by synergism of WNT signalling and *Tbx6*. *EMBO Rep.* 8, 784–789.
- Yoon, J.K., and Wold, B. (2000). The bHLH regulator pMesogenin1 is required for maturation and segmentation of paraxial mesoderm. *Genes Dev.* 14, 3204–3214.

STAR★METHODS

KEY RESOURCES TABLE

REAGENT or RESOURCE	SOURCE	IDENTIFIER
Chemicals, Peptides, and Recombinant Proteins		
CHIR99021	Axon Medchem	Cat#Axon1386
DAPT	Sigma-Aldrich	Cat#D5942
IWP-2	Sigma-Aldrich	Cat#I0536
DMEM/F12 without Glucose, Pyruvate, Phenol Red	Cell Culture Technologies	N/A
Penicillin/Streptomycin	Thermo Fisher Scientific	Cat# 15140122
D-Luciferin	Sigma-Aldrich	Cat#L9504
Cascade Blue	Life Technologies	Cat#C3239
Sylgard 184	Dow Corning	N/A
Fibronectin	Sigma-Aldrich	Cat#F1141
Experimental Models: Organisms/Strains		
Mouse: LuVeLu:CD1-Tg(Lfng-YFP/PEST)OP	Aulehla et al., 2008	N/A
Mouse: MESP2-GFP: ICR.Cg-Mesp2 ^{tm(GFP)} /YsaRbrc	Morimoto et al., 2006	Bioresources of Riken BRC RBRC:01862 RRID:IMSR_RBRC01862
Mouse: Axin2T2A-Luciferase: Axin2 ^{tm2.1(T2ALuciPEST)AAU}	This paper	N/A
Mouse: Axin2T2A: Axin2 ^{tm1(T2AVenusPEST)AAU}	This paper	N/A
Mouse: Lfng-T2A-Venus: Lfng ^{tm1.1(T2AVenusPEST)AAU}	This paper	N/A
Mouse: Hes7 Knockout: ICR.Cg-Hes7 ^{tm1Kag}	Bessho et al., 2001	Bioresources of Riken BRC RBRC:05983
Software and Algorithms		
Fiji	Schindelin et al., 2012	https://fiji.sc/ ; RRID: SCR_002285
MATLAB	Mathworks	https://de.mathworks.com/products/matlab.html ; RRID: SCR_001622
shadedErrorBar (MATLAB function)	Rob Campbell	https://de.mathworks.com/matlabcentral/fileexchange/26311-raacampbell-shadederrorbar
dScatter (MATLAB function)	Robert Henson (Eilers and Goeman, 2004)	https://www.mathworks.com/matlabcentral/fileexchange/8430-flow-cytometry-data-reader-and-visualization
R	N/A	https://www.r-project.org/about.html
LombScargle (R algorithm)	Glynn et al., 2006	N/A
Other		
LSM 780 laser-scanning microscope (Objective Plan-Apochromat 20x/0.8)	Zeiss	N/A
MZ16F stereo microscope with DFC420C digital camera	Leica	N/A
LV200 microscope (Objective PlanSApo 40x/0.9)	Olympus	N/A

CONTACT FOR REAGENT AND RESOURCE SHARING

Further information and requests for resources and reagents should be directed to and will be fulfilled by the Lead Contact, Alexander Aulehla (aulehla@embl.de).

EXPERIMENTAL MODEL AND SUBJECT DETAILS

Mouse lines

Axin2T2A and LfngT2A knockin reporter lines were generated employing standard gene targeting techniques using R1 embryonic stem cells.

To generate Axin2T2A alleles, we targeted the stop codon of the endogenous Axin2 locus with a reporter cassette coding for a destabilized fluorophore (Axin2T2AVenus-PEST, Axin2T2A) or a destabilized firefly luciferase (Axin2T2A-Luciferase-PEST, Axin2T2A-Luci). The reporter cassette is separated from the Axin2 gene via a 2A-site and includes a selection cassette. After generation of the knockin reporter line, the selection cassette was removed by Cre-mediated excision to yield the final Axin2T2A allele.

The LfngT2A allele was obtained by targeting the stop codon of the endogenous Lfng locus, the targeting construct contained one selection and two different reporter cassettes. The reporter cassettes were flanked by *frt*- and *loxP*-sites in a way that Cre-mediated excision of the selection cassette resulted in the LfngT2A allele in which the endogenous sequence coding for Lfng is followed by sequences coding for the destabilized fluorophore mVenus-PEST. The Mesp2-GFP line (Morimoto et al., 2006) was obtained from the RIKEN BRC through the National Bio-Resource Project of the MEXT, Japan. The Hes7-knockout line (Bessho et al., 2001) was provided by Yasumasa Bessho. The LuVeLu line was published previously (Aulehla et al., 2008). For all experiments (unless stated otherwise) female mice were sacrificed on 10.5 dpc and embryos dissected. All animal experiments were conducted under veterinarian supervision and after project approval by European Molecular Biology Laboratory, following the guidelines of the European Commission, Directive 2010/63/EU and AVMA Guidelines 2007.

METHOD DETAILS

Transgenesis, mouse strains and animal work

In vivo culture and *ex vivo* assays were performed as described previously (Lauschke et al., 2013). The following small molecule inhibitors dissolved in DMSO were used at the concentrations indicated in the text and Figure legends: CHIR99021 (“Chiron,” Axon Medchem), DAPT (Sigma-Aldrich) and IWP-2 (Sigma-Aldrich). For experiments including Hes7-knockout mice (Bessho et al., 2001), individual embryos were genotyped by PCR using primers 5'-AGAAAGGGCAGGGAGAAGTGGGCGAGCCAC-3', 5'-GTCTGTGAGAGCGAGAGGGGGTCTGGGATGG-3' and 5'-TTGGCTGCAGCCCCGGGGATCCACTAGTTC-3'.

mPSM *ex vivo* culture on microfluidic chip

Standard soft lithography techniques (El Debs et al., 2012) were applied for fabrication of microfluidic chips from polydimethylsiloxane (PDMS, Sylgard 184, Dow Corning). The structured side of the PDMS chip was treated with oxygen plasma and bonded to a glass slide (Marienfeld, High Precision No. 1.5H).

Microfluidic chips were coated with Fibronectin (Sigma-Aldrich, 1:20 in PBS) over night. Posterior PSM was dissected from E10.5 embryos and injected into microfluidic chips. The tissue was cultured on microfluidic chip with a constant flow rate of 60 μ l/h in humid atmosphere at 5% CO₂ and 37°C. Approximately after 1-2 h of cultivation in culture medium, pumping program to induce drug pulses was started (using either WPI Aladdin-1000 syringe pumps or computer-controlled Elveflow OB1 flow controller with flow sensors). Samples were excluded from further analysis, if the explant cultures primarily spread along the roof of the microfluidic chip or if cultures spread with the cut surface facing up.

In situ hybridization

Probe generation and *in situ* hybridization were described previously (Aulehla et al., 2003; Lauschke et al., 2013). Probes against Axin2, Uncx4.1 and Mesp2 were used as described in the literature (Aulehla et al., 2003; Mansouri et al., 1997; Saga et al., 1997). Probe against Venus was generated using a previously published plasmid (Nagai et al., 2002). Probe against Ripply2 was generated using the full-length cDNA (Morimoto et al., 2007).

Images of *in situ* hybridizations were taken with a Leica MZ16F stereo-microscope and a Leica DFC420C digital camera. Brightness and contrast were adjusted uniformly to the entire image.

Laser scanning microscopy

Imaging was performed using a Zeiss LSM780 laser-scanning microscope featuring an incubator for CO₂ and temperature control. Samples were excited with a Ti:Sapphire Laser (Chameleon-Ultra, Coherent) at a wavelength of 960 nm or an Argon laser at 514 nm (LuVeLu, Axin2T2AVenus and LfngT2AVenus) or 488 nm (Mesp2-GFP) through a 20x plan apo objective (numerical aperture 0.8). Every 10 min a z stack of either 6–8 planes (for *in vivo* imaging) or 3 planes (for *ex vivo* assay) at 8 μ m distance was scanned. Multiple samples were recorded using a motorized stage during each experiment. Movies were recorded in 512 \times 512 pixels, 1.38 μ m per pixel. Cascade Blue within microfluidic chamber was excited with 405 nm laser diode and a single z plane was detected every 10 min (32 \times 32 pixel, 22.14 μ m per pixel). For imaging of microfluidic experiments a Zeiss VBA macro (Microscopy PipelineConstructor) developed by the group of Jan Ellenberg, EMBL Heidelberg, was used (www.ellenberg.embl.de/index.php/software/microscopyautomation).

Bioluminescence imaging

For bioluminescence imaging *ex vivo* assays were cultured in 0.1 mM D-Luciferin (Sigma-Aldrich) on Fibronectin-coated glass-bottom dishes (MatTek). Simultaneous imaging of Axin2T2A-Luci and LuVeLu was performed with an Olympus LV200 microscope

equipped with a 40x PlanSApo objective (numerical aperture 0.9) and CO₂/ temperature control. LuVeLu was excited using an LED lamp (X-Cite XLED1, Excelitas) at 5%. Every 10 min an image was taken (exposure times: bioluminescence 9 min, LuVeLu 10 s).

QUANTIFICATION AND STATISTICAL ANALYSIS

Image and data processing

Quantification of oscillation dynamics were performed as described previously (Lauschke et al., 2013). For generation of fluorescence intensity kymographs Fiji (Schindelin et al., 2012), for determination of main period R and for the other processing steps MATLAB were used.

Generation and analysis of kymographs

To visualize Axin2T2A and Mesp2 polarity in somites (Figures 1C and 1G), Z-slices were subjected to a maximum intensity projection and time series were further processed with a Gaussian filter (5 μ m). Kymographs were generated along a user-defined line from posterior to anterior of mPSM cultures using the Fiji (Schindelin et al., 2012) plugin KymoResliceWide (intensity averaged over the width of a 50 px wide line) and then further smoothed using a Gaussian filter (5 μ m).

For the analysis of oscillation dynamics, kymographs were generated in the following way: After maximum intensity projection of all z-planes, time series were blurred using a Gaussian filter (10 μ m). Kymographs were generated along a user-defined line from posterior to anterior of mPSM cultures. Kymographs were blurred using a Gaussian filter (10 μ m sigma radius). Main period in posterior mPSM was determined along a line within a fluorescence intensity kymograph using the LombScargle algorithm (Glynn et al., 2006).

For quantification of time until onset of oscillation arrest (Figures 6A and 6C) or Mesp2-GFP expression (Figures S6C–S6H) time starting 3 h after dissection of embryos was taken into account.

Phase kymographs were generated as described previously (Lauschke et al., 2013).

Wave slopes were measured by manually defining their posterior starting points based on phase kymographs. For each wave, phases between 0.6π and 1π were considered and a regression line was calculated automatically (MATLAB). For numerical reason, the inverse slope was computed. Inverse wave velocities were derived from the slope of the regression line according to $velocity^{-1} = t/s * k$, with k being the slope of the regression line, s and t being the spatial and temporal resolution per pixel, respectively.

Analysis of simultaneous imaging of Axin2T2A-Luci and LuVeLu

Images were processed using the Fiji (Schindelin et al., 2012) plugin Remove Outliers (4 px) prior to fluorescence intensity kymograph generation (for kymograph generation see above). Kymographs were then detrended along the time coordinate (by subtraction of moving average-smoothened signal (window 15) from the original signal) and smoothed using a moving average function (window 5).

Analysis of entrainment of oscillations in anterior mPSM

Axin2T2A and LuVeLu reporter activity was quantified in the anterior mPSM region prior to oscillation arrest (see Figure 3C). Mean amplitude was calculated using Hilbert transform of detrended oscillation signals (Pikovsky et al., 2001).

For the analysis of synchronization, independent experiments were aligned to each other relative to the external force. To visualize synchronization between samples in time-series data, signals were normalized to the maximum value of each sample in the second half of an experiment (time points 65–120). Average and standard deviation of multiple samples were plotted using the MATLAB function `shadedErrorBar` (by Rob Campbell, MathWorks File Exchange).

Phases of reporter oscillations were determined using the Hilbert transform (Pikovsky et al., 2001). Phases of external force were set to 0 for the start of a drug pulse and then varied linearly between π and $-\pi$. Phase-phase plots were generated using the MATLAB function `dscatter` (by Robert Henson, MathWorks File Exchange, based on (Eilers and Goeman, 2004)). For generation of LuVeLu-Axin2T2A phase-phase plots (Figures 5C and 5G) oscillation phases of individual samples were randomly aligned to each other.

For statistical comparisons between groups, two-tailed Student's t tests were computed in Excel (Microsoft) (unequal variance for comparison between Axin2T2A and LuVeLu oscillations dynamics, otherwise equal variance).

DATA AND SOFTWARE AVAILABILITY

MATLAB scripts are available upon request.

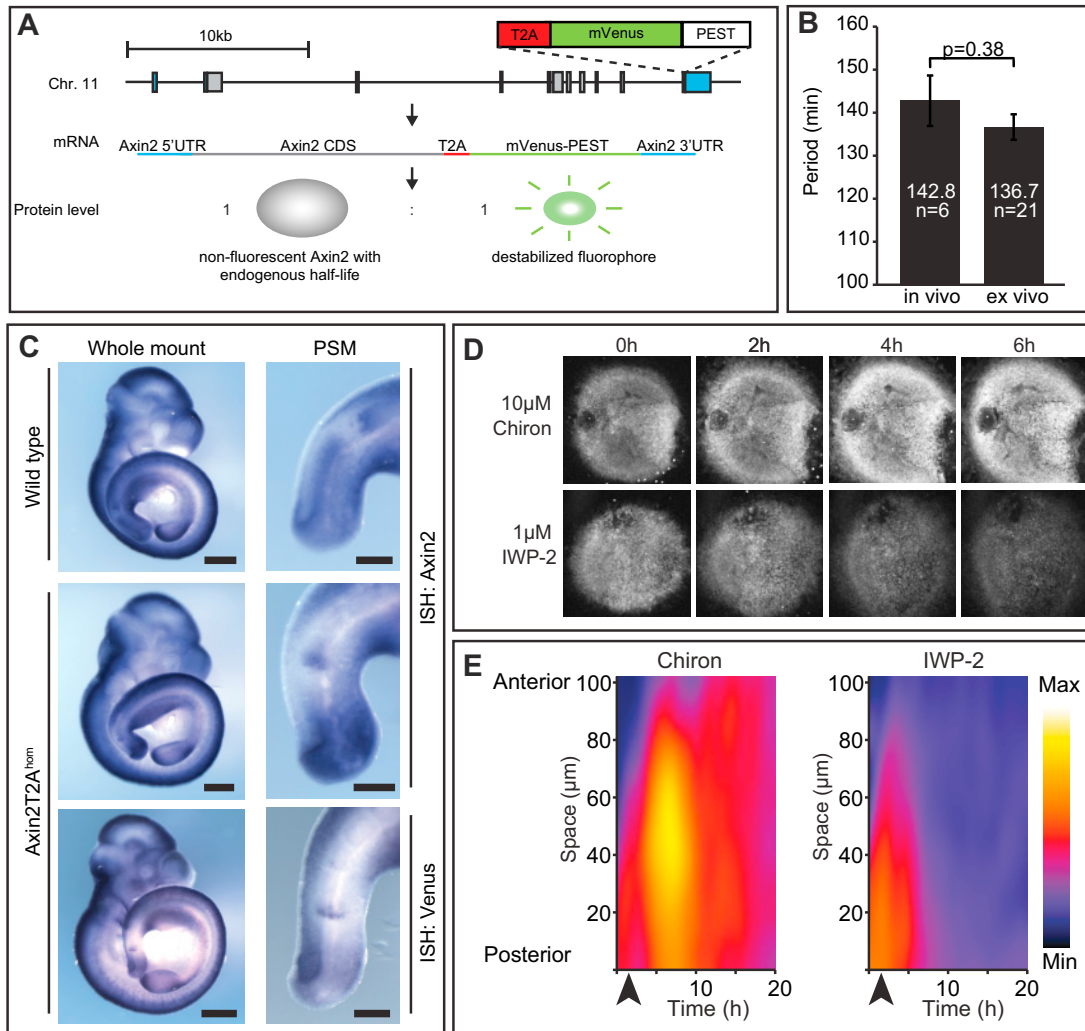


Figure S1. Real-Time Visualization of Wnt Signaling Oscillations during Mesodermal Patterning, Related to Figure 1

(A) Schematic depiction of Axin2T2A reporter strategy. Note that Axin2 coding sequences and endogenous untranslated regions (UTR) remain unaffected. Exons coding for untranslated regions are indicated in blue, exons corresponding to the protein coding sequence are shown as gray boxes.

(B) Quantification of Axin2T2A oscillation periods in *in vivo* experiments and *ex vivo* cell culture assays reveals no significant difference ($p = 0.38$). Error bars indicate SEM.

(C) *In situ* hybridization analysis against Axin2 transcripts reveals comparable expression patterns and transcript abundances in control embryos and embryos homozygous for the targeted Axin2T2A allele. In addition, Venus expression in Axin2T2A embryos corresponds to Axin2 expression patterns. Scale bar, 500 μm (whole mount embryos); scale bar, 200 μm (PSM).

(D) Time series of real-time imaging experiments showing *ex vivo* cultures treated with the Wnt agonist CHIR99021 (Chiron) or the Wnt antagonist IWP-2 ($n = 9/9$ for Chiron and $n = 5/5$ for IWP-2).

(E) Fluorescence intensity kymograph of Chiron-treated sample shown in (D) illustrates an increase in Axin2T2A fluorescence (left panel). Fluorescence intensity kymograph of IWP-2-treated sample shown in (D) reveals persistent decrease of Axin2T2A signal (right panel). Fluorescence intensity is color-coded.

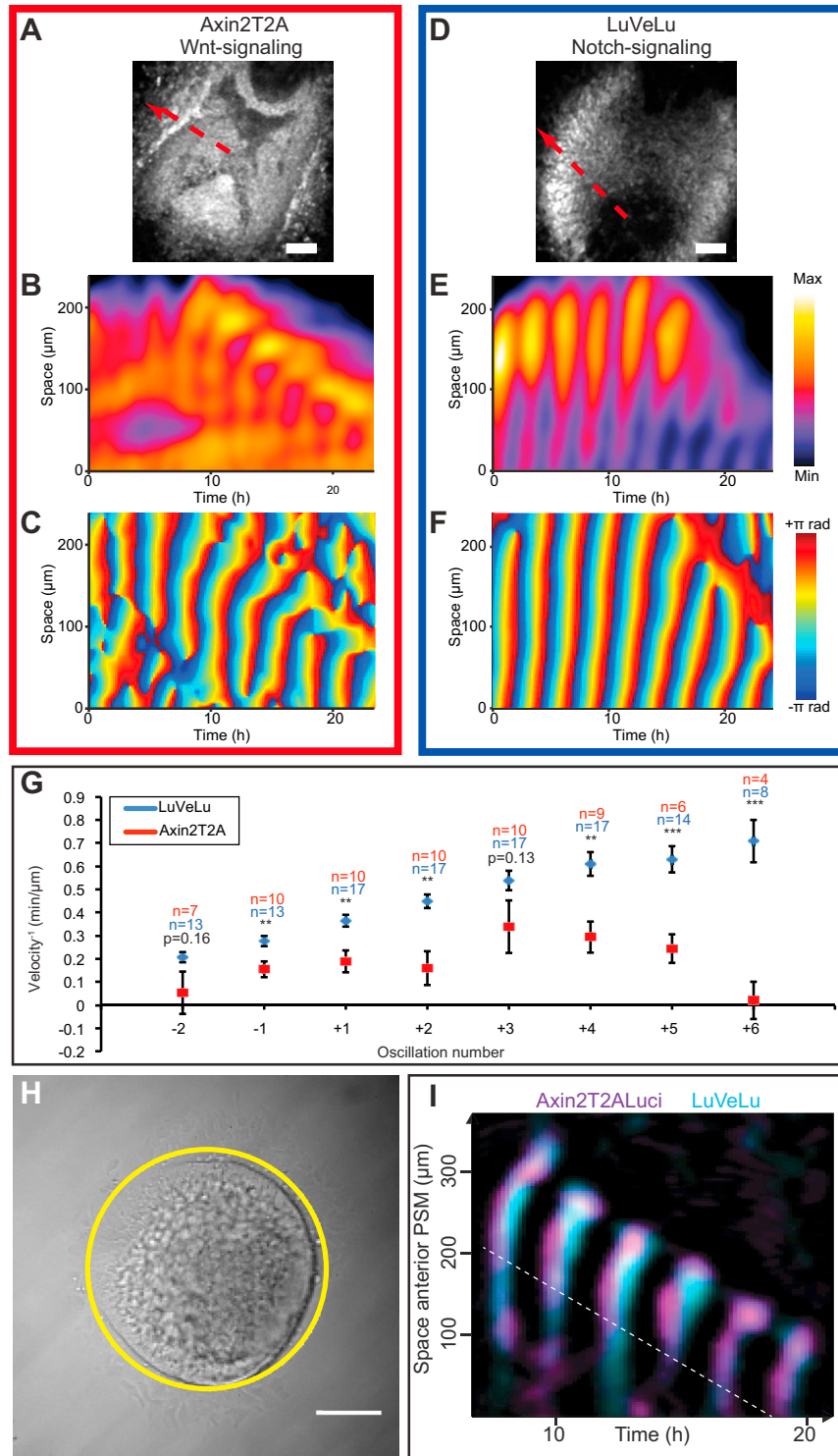


Figure S2. Phase Shift between Wnt and Notch Signaling Oscillations Differs between Posterior and Anterior mPSM, Related to Figure 2
 (A-G) Comparison of Wnt and Notch signaling reporter oscillations. *Ex vivo* cell culture assays using Wnt reporter Axin2T2A (A-C, boxed in red) or Notch reporter LuVeLu (D-F, boxed in blue) were analyzed. Dashed red arrows in A and D depict lines along which the fluorescence intensity kymographs (B,E) were generated (the same kymographs are also shown in Figures 2A and 2B). Fluorescence intensity is color-coded individually for both kymographs. Oscillation phases were calculated and plotted in phase kymographs (C,F). Oscillation phase values from $-\pi$ rad to $+\pi$ rad are color-coded. Note the differences in oscillation kinetics between the biphasic Axin2T2A (C) and the LuVeLu (F) profile.

(legend continued on next page)

(G) Based on LuVeLu and Axin2T2A phase kymographs, respectively, inverse velocity of signaling waves was measured and plotted against corresponding oscillation number (waves were numbered relative to the onset of segment formation in 2D *ex vivo* assay (Lauschke et al., 2013)). Error bars indicate s.e.m, ** $p < 0.01$, *** $p < 0.001$.

(H) In posterior PSM cells Axin2T2A-Luci and LuVeLu oscillate out-of-phase. Representative brightfield image of *ex vivo* mPSM culture using Axin2T2A-Luci/LuVeLu double-positive embryo at beginning of culture. Note that only posterior PSM cells are used to generate *ex vivo* cultures, so that oscillations detected at beginning of cultivation period represent exclusively posterior PSM cells (Lauschke et al., 2013). Scale bar, 100 μm . Quantification of reporter activity in region of interest (yellow circle) is shown in Figure 2E.

(I) Detrended, normalized intensity kymograph of simultaneous imaging of anterior region of *ex vivo* assay using Axin2T2A-Luci (magenta) and LuVeLu (cyan) double-positive samples. Quantification of reporter oscillations along dashed line is shown in Figure 2F.

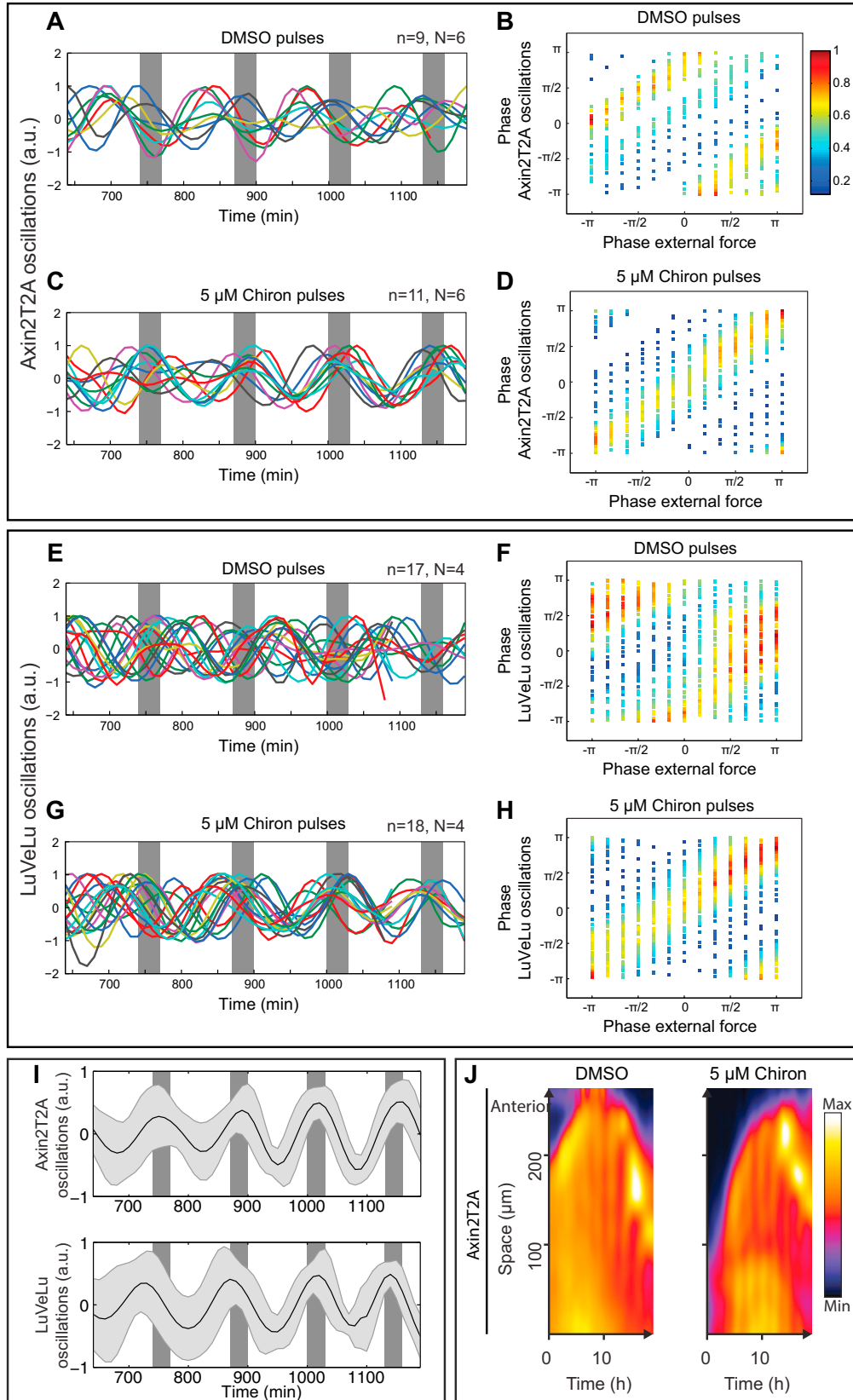


Figure S3. Entrainment of the Segmentation Clock to Pulses of 5 μ M Chiron, Related to Figures 3 and 4

(A–D) Entrainment of Axin2T2A oscillations to periodic pulses of the canonical Wnt signaling agonist CHIR99021 (Chiron, 5 μ M):

(A and C) Quantification of (detrended, normalized) Axin2T2A signal in anterior mPSM reveals oscillations in control (A) and Chiron-treated samples (C). Experiments (N = independent experiments, n = individual samples) were combined using the external force (gray bars) as an objective time reference.

(B and D) Phase-phase plots of the phase-relation between endogenous rhythm (Axin2T2A) and external periodic force (control: DMSO pulses (B), treatment: Chiron pulses (D)). Density of points within the plots is color-coded.

(E–H) Entrainment of LuVeLu oscillations to periodic pulses of the Wnt signaling activator Chiron (5 μ M):

(E and G) Quantification of (detrended, normalized) LuVeLu signal in anterior mPSM reveals oscillations in control (E) and Chiron-treated samples (G). Experiments (N = independent experiments, n = individual samples) were combined using the external force (gray bars) as an objective time reference.

(F and H) Phase-phase plots of the phase-relation between endogenous rhythm (LuVeLu) and external periodic force (control: DMSO pulses (F), treatment: Chiron pulses (H)). Density of points within the plots is color-coded.

(I) Mean reporter activity (black line) and s.d. (gray shading) of Axin2T2A oscillations shown in (C) and LuVeLu oscillations shown in (G) reveal in-phase oscillations in anterior mPSM upon entrainment with Chiron pulses (N = independent experiments, n = individual samples).

(J) Representative Axin2T2A fluorescence intensity kymographs of DMSO control- (left panel) and Chiron-treated mPSM *ex vivo* cultures (right panel). Fluorescence intensity is color-coded.

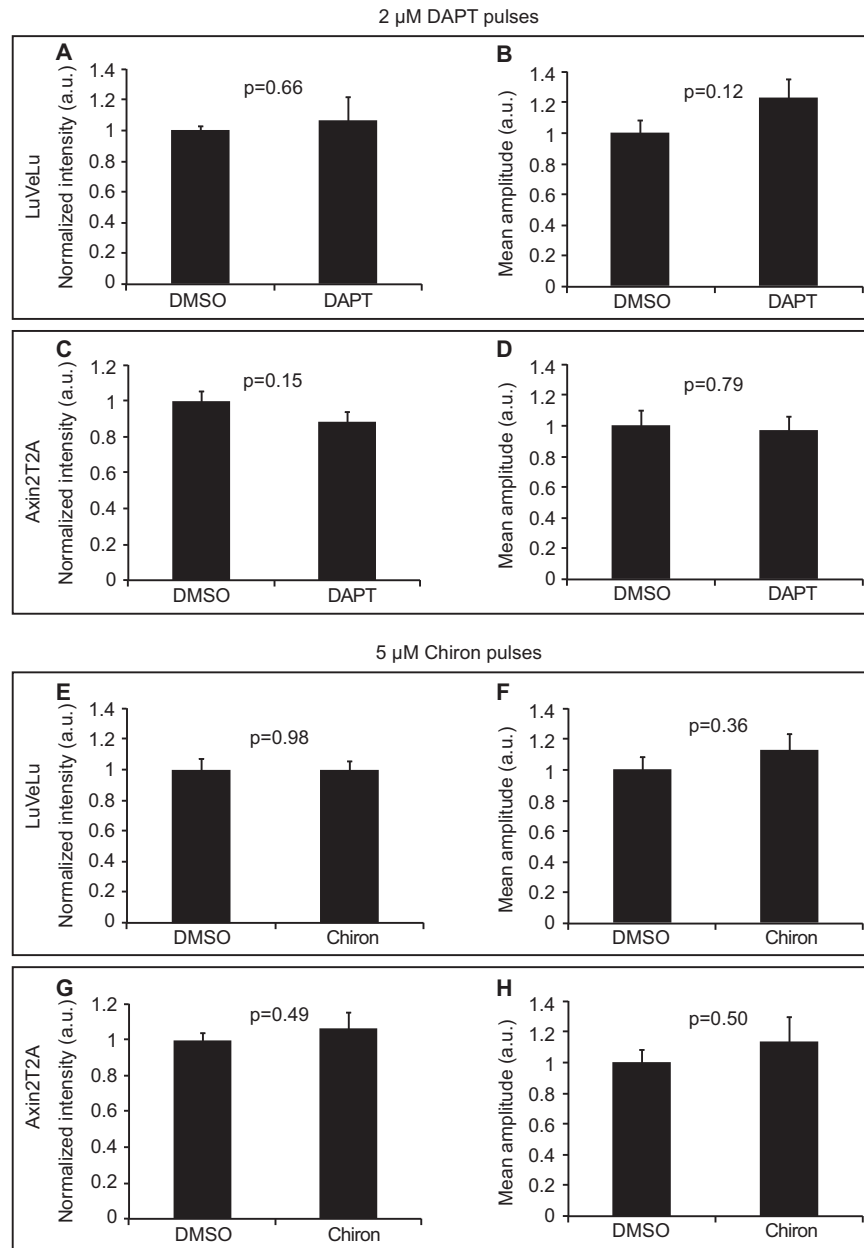


Figure S4. Single-Drug Pulses of Either DAPT or Chiron Do Not Significantly Alter Absolute Intensity or Mean Amplitude of LuVeLu and Axin2T2A Oscillations in Anterior mPSM, Related to Figures 3, 4, and S3

Quantification of LuVeLu and Axin2T2A signals in anterior mPSM of *ex vivo* assays cultured with pulses of 2 μ M DAPT (A-D) or 5 μ M Chiron (E-H). Mean intensity of LuVeLu (A,E) or Axin2T2A (C,G) reporter signal and mean amplitude of LuVeLu (B,F) or Axin2T2A (D,H) reporter oscillations were determined. DAPT or Chiron-treated samples, respectively, were quantified relative to DMSO-treated samples. Quantifications are based on time points 50 to 120 to exclude beginning of *ex vivo* culture, when anterior mPSM region has not re-established yet (Lauschke et al., 2013). Error bars denote SEM.

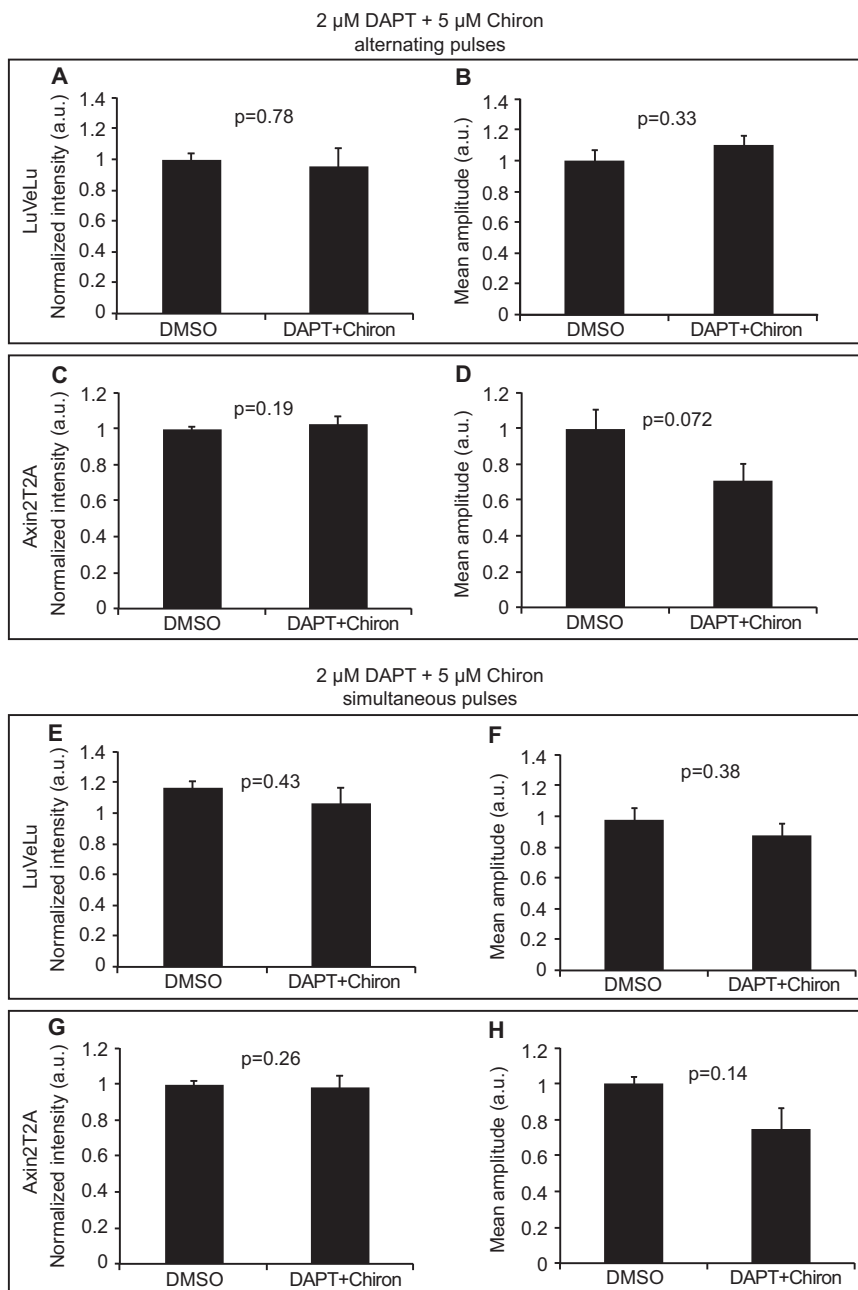


Figure S5. Alternating or Simultaneous Pulses of DAPT and Chiron Do Not Significantly Change Absolute Intensity or Mean Amplitude of LuVeLu and Axin2T2A Oscillations in Anterior mPSM, Related to Figure 5

(A–H) Quantification of LuVeLu and Axin2T2A signals in anterior mPSM of *ex vivo* assays cultured with alternating (A–D) or simultaneous pulses (E–H) of 2 μ M DAPT and 5 μ M Chiron. Mean intensity of LuVeLu (A and E) or Axin2T2A (C and G) reporter signal and mean amplitude of LuVeLu (B and F) or Axin2T2A (D and H) reporter oscillations were determined. DAPT/Chiron-treated samples were quantified relative to DMSO-treated samples. Quantifications are based on time points 50 to 120 to exclude beginning of *ex vivo* culture, when anterior mPSM region has not re-established yet (Lauschke et al., 2013). Error bars denote SEM.

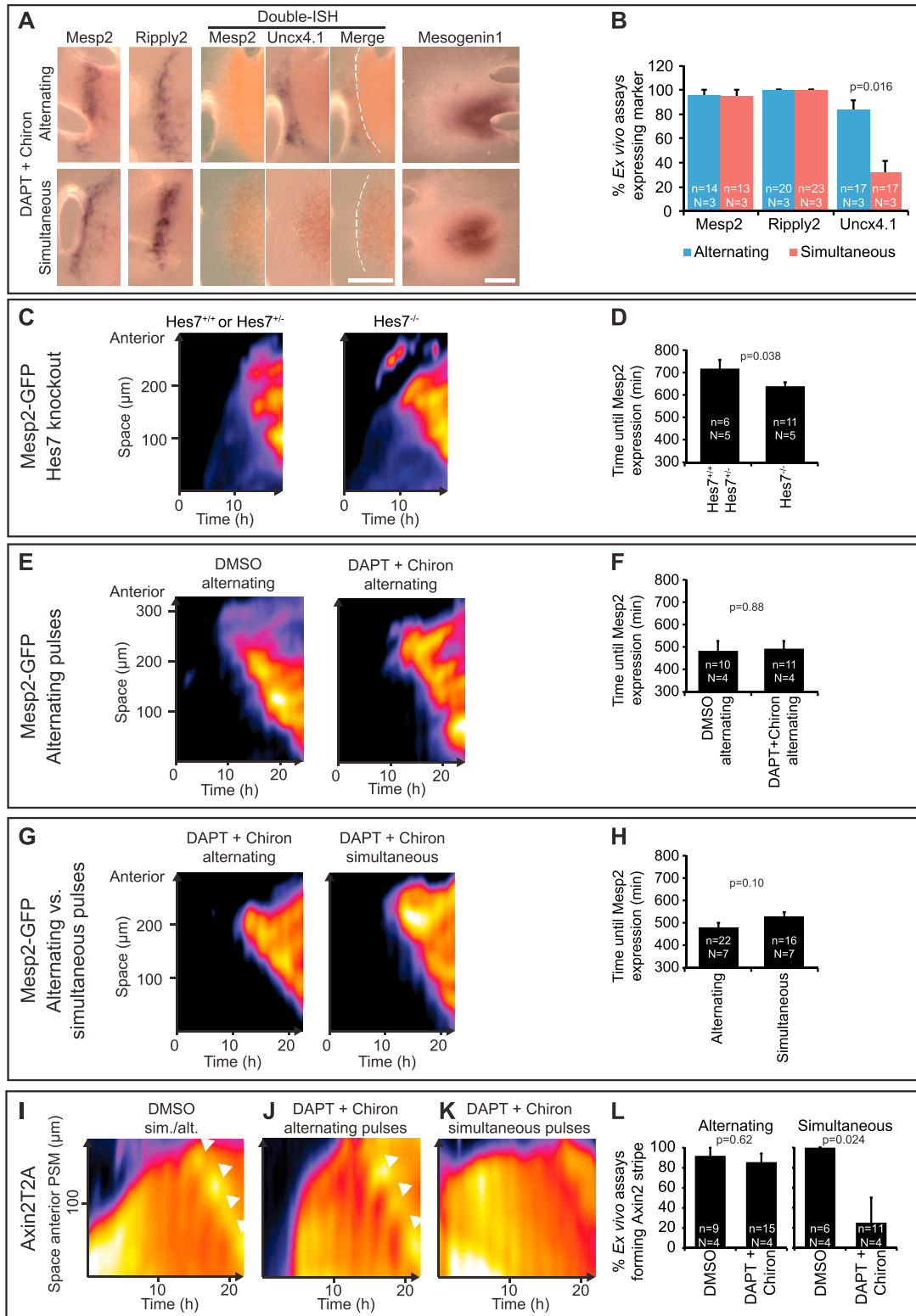


Figure S6. Effect of Anti-phase Wnt and Notch Signaling Oscillations on Segmentation, Related to Figure 6

(A and B) Molecular analysis of segmentation marker expression upon altered Wnt/Notch phase shift. (A) *Ex vivo* cultures were treated with either alternating or simultaneous pulses of DAPT and Chiron. Samples were fixed after 18 h of culture and subjected to *in situ* hybridization using probes against the indicated mRNAs. Representative images are shown. (B) Percentage of *ex vivo* cultures expressing Mesp2, Ripply2 and Uncx4.1 was quantified.

(legend continued on next page)

(C and D) Quantification of Mesp2-GFP reporter activity in *ex vivo* mPSM cultures either in the presence or absence of the transcriptional repressor Hes7. (C) Representative fluorescence intensity kymographs of samples generated from Hes7-expressing (Hes7^{+/+} or Hes7^{+/-}, left panel) or Hes7-knockout embryos (Hes7^{-/-}, right panel). (D) Quantification of time until onset of Mesp2-GFP expression is depicted.

(E and F) Quantification of Mesp2-GFP reporter activity in *ex vivo* mPSM cultures treated with alternating pulses of DMSO or pulses of 2 μ M DAPT and 5 μ M Chiron. (E) Representative fluorescence intensity kymographs for DMSO- (left panel) or DAPT/Chiron-treated samples (right panel). (F) Quantification of time until onset of Mesp2-GFP expression is shown.

(G and H) Quantification of Mesp2-GFP reporter activity in *ex vivo* mPSM cultures treated with either alternating or simultaneous pulses of 2 μ M DAPT and 5 μ M Chiron. (G) Representative fluorescence intensity kymographs for samples treated with alternating (left panel) or simultaneous DAPT/Chiron pulses (right panel). (H) Quantification of time until onset of Mesp2-GFP expression is shown.

(I–L) Induction of Axin2T2A expression in posterior segment halves in anterior mPSM is prevented by anti-phase Wnt/Notch oscillations. Representative fluorescence intensity kymographs of *ex vivo* cultures treated either with DMSO (I) or alternating DAPT and Chiron pulses (J) are shown. In contrast, the anterior Axin2 expression domain was absent in samples entrained with simultaneous pulses of DAPT and Chiron (K). (L) Quantification of *ex vivo* cultures showing Axin2 stripe in anterior mPSM. Fluorescence intensity in kymographs is color-coded. Error bars denote SEM.